17- and 19-Electron Complexes $[Fe^{III}(\eta^5\text{-}C_5R_5)(S_2CNMe_2)L]^{n+}$ ($n = 1, 0$): Electronic Structure and Substitution and Redox Chemistry. Formation of $[Fe^{IV}(\eta^5\text{-}C_5R_5)(dtc)_2]$ and Characterization of both 17e and 19e States of a Transition-Metal Complex

Marie-Hélène Delville-Desbois,*,† Stefan Mross,† Didier Astruc,*,† Jorge Linares,‡ François Varret,*,‡ Hassan Rabaâ,§,|| Albert Le Beuze,§ Jean-Yves Saillard,*,§ Robert D. Culp,⊥ David A. Atwood,⊥ and Alan H. Cowley*,⊥

Contribution from the Laboratoire de Chimie Organique et Organométallique, URA CNRS No. 35, Université Bordeaux I, 351 Cours de la Libération, 33405 Talence Cédex, France, Département de Recherches Physiques, URA CNRS No. 71, Université P. et M. Curie, Tour 22, 4 Place Jussieu, 75252 Paris Cédex 05, France, Laboratoire de Chimie du Solide et Inorganique Moléculaire, URA CNRS No. 495, Université de Rennes I, Campus de Beaulieu, 35042 Rennes Cédex, France, Laboratoire de Chimie Théorique, Faculté des Sciences, Université Ibn Tofail, BP 133, Kénitra, Morocco, and Department of Chemistry and Biochemistry, The University of Texas at Austin, Austin, Texas 78712-1167

Received October 27, 1995[⊗]

Abstract: Oxidation of $[FeCp^*(\eta^1\text{-dtc})(CO)_2]$, **1** ($Cp^* = \eta^5\text{-}C_5Me_5$, dtc = S_2CNMe_2), or $[FeCp^*(\eta^2\text{-dtc})(CO)]$, **2**, using $[Fe^{III}Cp_2]^+X^-$ ($X^- = PF_6^-$ or BF_4^-, $Cp = \eta^5\text{-}C_5H_5$) in THF cleanly gives $[Fe^{III}Cp^*(\eta^2\text{-dtc})(CO)]^+X^-$, $\mathbf{2}^+\mathbf{X}^-$, as microcrystalline green, thermally stable, but substitution labile, salts. The substitution of CO in $\mathbf{2}^+\mathbf{PF_6}^-$ by various solvents (CH_2Cl_2, THF, CH_3COCH_3, CH_3CN) (visible spectroscopy) follows pseudo-first-order kinetics but shows clearly the influence of the incoming solvent ligand on the substitution rate and, hence, is in good agreement with an associative mechanism. Displacement of the labile solvent ligand in these complexes by a phosphine results in the 17-electron (17e) cations $[Fe^{III}Cp^*(\eta^2\text{-dtc})(L)]^+PF_6^-$, L = PPh_3 ($\mathbf{7}^+\mathbf{PF_6}^-$) or η^1-dppe ($\mathbf{8}^+\mathbf{PF_6}^-$). The same reaction in the presence of the anionic ligands CN^-, SCN^-, and Cl^- affords the corresponding neutral 17e Fe^{III} complexes (respectively compounds **11**, **13**, and **14**). All these 17e complexes were characterized by IR, ESR, and Mössbauer spectroscopies and elemental analysis. The cations were reduced to isostructural neutral Fe^{II} complexes using 1 equiv of $[Fe^ICp(C_6Me_6)]$ in THF or oxidized to the robust green 18e Fe^{IV} complex $[Fe^{IV}(\eta^5\text{-}C_5Me_5)(\eta^2\text{-}S_2CNMe_2)_2]^+$-$PF_6^-$, $\mathbf{9}^+\mathbf{PF_6}^-$, using $Na^+dtc^-\cdot 2H_2O$. $[Fe^{IV}(\eta^5\text{-}C_5(CH_2C_6H_5)_5)(\eta^2\text{-}S_2CNMe_2)_2]^+PF_6^-$, $\mathbf{16}^+\mathbf{PF_6}^-$, was structurally characterized, and the dihapto mode of coordination of both dtc ligands was established. The 19e Fe^{III} species **9** was shown to be an intermediate which further reduced H_2O. It could be alternatively synthesized by reduction of the 18e precursor $\mathbf{9}^+\mathbf{PF_6}^-$ using 1 equiv of $[Fe^ICp(C_6Me_6)]$ or by addition of anhydrous Na^+dtc^- to $\mathbf{3}^+\mathbf{PF_6}^-$ in MeCN at −40 °C. The 19e complex **9** showed an ESR spectrum indicating an axial symmetry (two *g* values) in contrast with the ESR spectra of all the 17e species ($\mathbf{2}^+$−**14**) which show three *g* values characteristic of a rhombic distortion (for instance, the very close model **13**). The Mössbauer doublet of **9** very slowly evolved to the new doublet of the thermally stable 17e complex **9′**. In MeCN solution, the transformation of the blue complex **9** to the purple 17e complex **9′** was much more rapid (above −40 °C) as indicated by the rhombic spectrum of **9′** in frozen solution and by low-temperature ^{13}C NMR. In toluene, however, the 19e complex **9** showed a remarkable stability up to room temperature, which allowed recording of the ^{13}C spectrum in d^8-toluene. MO calculations have been performed on models for the 17e and 19e bis-dtc Fe^{III} complexes. They suggest that the 17e species should have some significant sulfur spin density. The 19e species is found to have its odd electron occupying an antibonding metal-centered orbital. The cyclic voltammogram of $\mathbf{9}^+\mathbf{PF_6}^-$ under continuous scanning for the monoelectronic reduction and the two monoelectronic reductions showed the decrease of the waves of $\mathbf{9}^+\mathbf{PF_6}^-$ and the concomitant increase of those due to the partially decoordinated dtc complexes formed upon reduction. This permits an interpretation of the CV in terms of a triple-square scheme involving $\mathbf{9}^{+/0/-}$, $\mathbf{9'}^{+/0/-}$, and solvent (DMF) adducts in 18- and 19e states.

Introduction

The factors controlling the thermodynamic and kinetic stability of 17e complexes[1,2] are of current interest because of the intermediacy of these species in redox catalysis and electrocatalysis.[3,4] Such types of catalysis involving electron transfer (ET) are used in energy conversion[5] and in multicatalytic devices.[6] In this context, the study of the 17e complexes containing the chelating dithiocarbamate ligand seemed timely

† URA No. 35.

‡ URA No. 71. Present address: Laboratoire d'Optique et de Magnétisme, URA No. 1531, Université de Versailles, 45 Avenue des Etats-Unis, 78035 Versailles Cedex, France. Mössbauer studies.

§ URA No. 495. Theoretical studies.

|| Université Ibn Tofail.

⊥ The University of Texas at Austin. X-ray crystal structures.

⊗ Abstract published in *Advance ACS Abstracts,* April 1, 1996.

(1) (a) *Organometallic Radical Processes*; Trogler, W. C., Ed.; Elsevier: New York; *J. Organomet. Chem. Lib.* **1990**, *22*. (b) *Paramagnetic Species in Activation Selectivity, Catalysis*; Chanon, M., Juliard, M., Poite, J. C., Eds.; Kluwer: Dordrecht, The Netherlands, 1988. (c) Astruc, D. *Electron Transfer and Radical Processes in Transition-Metal Chemistry*; VCH: New York, 1995.

S0002-7863(95)03603-1 CCC: $12.00

in view of the potential electron-reservoir property[7] of the delocalized iron−η^2-dithiocarbamate (dtc) metallocyclic fragment.[8,9] It was hoped that this ligand would stabilize organoiron radicals. With this system, we have disclosed the first example of an electrocatalyzed reaction which can be initiated either by an oxidant[4b,10a,b] or by a reductant:[10c]

$$\underset{\mathbf{1}}{[FeCp^*(\eta^1\text{-dtc})(CO)_2]} \xrightarrow{\pm e \text{ or } h\nu} \underset{\mathbf{2}}{[FeCp^*(\eta^2\text{-dtc})(CO)]} + CO \quad (1)$$

Since the major problem in these ET chains is, as in organic chemistry,[11] the side reactions of the intermediate radicals,[3c] we attempted to isolate, characterize, and study the chemistry of such radicals.[12] A number of 17e complexes are already known,[2] but no examples featuring the dtc ligand have been reported before this study.[12] The chemistry presented here is rich and permits novel features of the 17e states to be elucidated. The parent 18e complexes $[FeCp(\eta^1\text{-dtc})(CO)_2]$ and $[FeCp(\eta^2\text{-dtc})(CO)]$ ($Cp = C_5H_5$) have been known for more than two decades, but we found the C_5Me_5 (Cp*) series easier to study,[9e] although still extremely labile in their 17e form. Complex **2** can also be obtained cleanly from **1** by visible-light photolysis[13] (eq 1) whereas both oxidatively and reductively induced electrocatalyzed chelations proceed in lower yields.[10a−c] In this article, we explore the access, electronic structure, stability, substitution lability, and redox processes of the 17e complexes $[Fe^{III}Cp^*(\eta^2\text{-dtc})(L)]^{x+}$ ($x = 0, 1$). Their transformation into the novel complexes $[FeCp^*(\eta^2\text{-dtc})_2]^{n+}$ (Fe^{III} for $n = 0$, Fe^{IV} for $n = 1$) is shown.[10d] When $n = 0$, one of the dtc ligands can be monodentate (17e) or bidentate (19e), which leads to the observation of an original transition-metal complex which can have either 17 or 19 valence electrons (VE).

Results and Discussion

Synthesis of the 17e Complexes $[Fe^{III}Cp^*(\eta^2\text{-dtc})(CO)]^+X^-$, $X^- = PF_6^-$ or BF_4^-. The reaction between 1 equiv of $[Fe^{III}Cp_2]^+X^-$, $X^- = PF_6^-$ or BF_4^-,[14] in THF suspension and 1 equiv of either the monodentate complex $[FeCp^*(\eta^1\text{-dtc})(CO)_2]$, **1**, or the bidentate complex $[FeCp^*(\eta^2\text{-dtc})(CO)]$, **2**, cleanly gives a yellow-orange solution containing $[FeCp_2]$ and an insoluble green powder. Attempts to solubilize and recrystallize this green powder always led to a rapid color change indicative of an evolution of this complex in solution. However, elemental analyses were satisfactory for the 1e oxidation products $\mathbf{2}^+\mathbf{X}^-$ ($X^- = PF_6^-$ or BF_4^-). The infrared spectra recorded from KBr pellets showed the presence of terminal CO stretches characteristic of the cationic nature of the complex ($\nu_{CO} = 2030$ and 1985 cm^{-1}); the presence of the dtc ligand in its chelate form[15] was suggested by the stretches corresponding to CN and CS bonds ($\nu_{CN} = 1550$ cm^{-1}, $\nu_{CS} = 1015$ cm^{-1}). The ESR spectra were consistent with an iron-centered radical and an orthorhombic−axial transition in the solid-state sample was observed at 200 K. The Mössbauer spectrum showed the parameters of Fe^{III} (IS = 0.518 mm s^{-1} vs Fe; QS = 0.686 mm s^{-1}) close to those obtained for the 17e Fe^{III} complexes $[Fe^{III}Cp^*(CO)(L)(CH_3)]^+PF_6^-$ or $[Fe^{III}Cp^*(CH_3)(L)_2]^+PF_6^-$ (L = phosphine).[17,18] Additional evidence for the formation of $\mathbf{2}^+\mathbf{PF_6}^-$ was provided by its monoelectronic reduction using $[Fe^{I}Cp(C_6Me_6)]$ in THF solution at 20 °C (15 min), a reaction which cleanly gave back the soluble complex **2** and a yellow precipitate of $[Fe^{II}Cp(C_6Me_6)]^+PF_6^-$ (Scheme 1).

Although the system $\mathbf{2}/\mathbf{2}^+\mathbf{PF_6}^-$ is not fully chemically reversible in THF solution because of the exchange of the CO ligand with THF in the presence of $[^nBu_4N^+]BF_4^-$, the thermodynamic potential ($E°$) is easily accessible (+0.605 V vs. SCE).[10a,d] As already shown,[10d] ferrocenium salts can quantitatively oxidize **2** even if the thermodynamic potential of the couple $FeCp_2/[FeCp_2]^+PF_6^-$ is only + 0.4 V vs. SCE.[2b] If we assume that the solution is homogeneous, the redox reaction (eq 2) is endergonic by 0.2 V (4.6 kcal/mol). However,

$$\mathbf{2} + [FeCp_2]^+PF_6^- \rightarrow \mathbf{2}^+\mathbf{PF_6}^- + FeCp_2 \qquad \Delta G = 4.6 \text{ kcal/mol} \quad (2)$$

in THF, neither $[FeCp_2]^+PF_6^-$ nor $\mathbf{2}^+\mathbf{PF_6}^-$ is soluble and the displacement of the redox equation in favor of the formation of $\mathbf{2}^+\mathbf{PF_6}^-$ must be driven by its greater insolubility in this solvent. Indeed, this complex is totally inert toward ligand exchange in this relatively apolar solvent. Addition of a salt, such as $[^nBu_4N^+]BF_4^-$, or a cosolvent, such as CH_2Cl_2 (3/1),

(2) For reviews, see Reference 1 and: (a) Baird, M. C. *Chem. Rev.* **1988**, *88*, 1217. (b) Connelly, N. G.; Geiger, W. E. *Adv. Organomet. Chem.* **1984**, *23*, 2. (c) Geiger, W. E.; Connelly, N. G. *Adv. Organomet. Chem.* **1985**, *24*, 87. (d) Stiegman, A. E.; Tyler, D. R. *Comments Inorg. Chem.* **1986**, *5*, 215. (e) Geoffroy, G. L.; Wrighton, M. S. "*Organometallic Photochemistry*; Academic Press: New York, 1979. (f) Meyer, T. J.; Caspar, J. V. *Chem. Rev.* **1985**, *85*, 187. (g) Brown, T. L. *Ann. N.Y. Acad. Sci.* **1980**, *331*, 80. (h) Kobayashi, T.; Yasufuku, K.; Iwai, I.; Yesaka, H.; Noda, H.; Ohtani, H. *Coord. Chem. Rev.* **1985**, *64*, 1.

(3) For reviews, see: (a) Kochi, J. K. *J. Organomet. Chem.* **1986**, *300*, 139. (b) Chanon, M. *Acc. Chem. Res.* **1987**, *20*, 214. (c) Astruc, D. *Angew. Chem., Int. Ed. Engl.* **1988**, *27*, 643.

(4) Hersgberger, J. W.; Klinger, R. J.; Kochi, J. K. *J. Chem. Soc., Chem. Commun.* **1982**, 212. (b) Hersgberger, J. W.; Klinger, R. J.; Kochi, J. K. *J. Am. Chem. Soc.* **1983**, *105*, 61. (c) Catheline, D.; Astruc, D. *Coord. Chem. Rev.* **1982**, *23*, 41.

(5) See for instance: Lehn, J. M.; Sauvage, J. P.; Ziessel, R. *Nouv. J. Chim.* **1979**, *3*, 423.

(6) Wrighton, M. S. *Comments Inorg. Chem.* **1985**, *4*, 269.

(7) Astruc, D. *Acc. Chem. Res.* **1986**, *19*, 377; *Comments Inorg. Chem.* **1987**, *6*, 61 (see also ref 1c, Chapter 6, and ref 3c).

(8) For reviews on dithiocarbamate complexes, see: (a) Fackler, J. P. *Adv. Chem. Ser.* **1976**, *No. 150*, 394. (b) Thorn, G. D.; Ludwig, R. A. *The Dithiocarbamates and Related Compounds*; Elsevier: Amsterdam, 1962. (c) Livingstone, S. E. *Q. Rev. Chem. Soc.* **1965**, *19*, 416. (d) Coucouvanis, D. In *Progress in Inorganic Chemistry*; Lippard, S., Ed.; Wiley: New York, 1970; Vol. 11, p 233. (e) Coucouvanis, D. *Prog. Inorg. Chem.* **1979**, *26*, 301. (f) Willemse, J.; Cras, J. A.; Steggarda, J. J.; Keijzers, C. P. *Struct. Bonding* (*Berlin*) **1976**, *28*, 83.

(9) For synthesis and studies of 18e [FeCp(dtc)] complexes, see: (a) O'Connor, C.; Gilbert, J. D.; Wilkinson, G. *J. Chem. Soc. A* **1969**, 84. (b) Cotton, F. A.; McCleverty, J. A. *Inorg. Chem.* **1964**, *5*, 1398. (c) Román, E.; Catheline, D.; Astruc, D.; Batail, P.; Ouahab, L.; Varret, F. *J. Chem. Soc., Chem. Commun.* **1982**, 129. (d) Román, E.; Astruc, D. *Inorg. Chem.* **1979**, *18*, 3284. (e) Catheline, D.; Román, E.; Astruc, D. *Inorg. Chem.* **1984**, *23*, 4508. (f) Román, E.; Catheline, D.; Astruc, D. *J. Organomet. Chem.* **1982**, *236*, 229.

(10) (a) Amatore, C.; Verpeaux, J.-N.; Madonik, A. M.; Desbois, M.-H.; Astruc, D. *J. Chem. Soc., Chem. Commun.* **1988**, 200. (b) Verpeaux, J.-N.; Desbois, M.-H.; Madonik, A. M.; Amatore, C.; Astruc, D. *Organometallics* **1990**, *9*, 630. (c) Desbois, M.-H.; Astruc, D. *J. Chem. Soc., Chem. Commun.* **1990**, 943; **1995**, 249. (d) Desbois, M.-H.; Astruc, D. *Angew. Chem., Int. Ed. Engl.* **1989**, *28*, 460.

(11) (a) Bunnett, J. F. *Acc. Chem. Res.* **1978**, *11*, 413. (b) Savéant, J.-M. *Acc. Chem. Res.* **1980**, *13*, 323.

(12) See ref 10a,b.

(13) Desbois, M.-H.; Nunn, C. M.; Cowley, A. H.; Astruc, D. *Organometallics* **1990**, *9*, 640.

(14) Catheline, D.; Astruc, D. *J. Organomet. Chem.* **1982**, *226*, C52.

(15) (a) Bonatti, F.; Hugo, R. *J. Organomet. Chem.* **1967**, *10*, 257. (b) Malatesta, L.; Bonatti, F. *Isocyanide Complexes of Metals*; Wiley: New York, 1969.

(16) Rajasekharan, M. V.; Giezynski, S.; Ammeter, J. H.; Ostwald, N.; Michaud, P.; Hamon, J.-R.; Astruc, D. *J. Am. Chem. Soc.* **1982**, *104*, 2400.

(17) Morrow, J.; Catheline, D.; Desbois, M. H.; Manriquez, J. M.; Ruiz, J.; Astruc, D. *Organometallics* **1987**, *6*, 2605.

(18) Greenwood, N. N.; Gibb, T. C. In *Mössbauer Spectroscopy*; Chapmann and Hall: London, 1971; Chapter 8 and references cited therein. See also this chapter for a few Fe^{IV} inorganic complexes.

(19) (a) Hamon, J.-R.; Astruc, D.; Michaud, P. *J. Am. Chem. Soc.* **1981**, *103*, 758. (b) Astruc, D.; Hamon, J.-R.; Lacoste, M.; Desbois, M.-H.; Román, E. *Organomet. Synth.* **1988**, *4*, 172.

Scheme 1

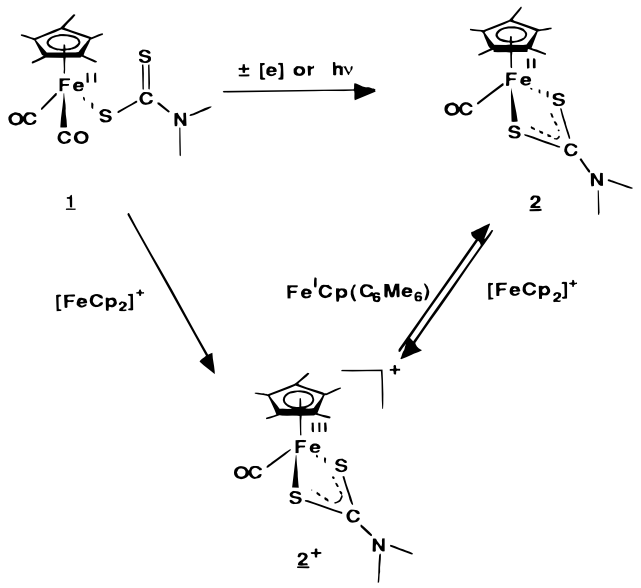

increases the polarity of THF, solubilizes $\mathbf{2}^+\mathbf{PF_6}^-$ in the medium, and leads to $\mathbf{4}^+\mathbf{PF_6}^-$ in which the last carbonyl group has been replaced by a THF molecule. This was confirmed by electrochemical experiments which revealed that, when **1** and **2** were oxidized electrochemically in THF on a preparative scale, they gave a brown salt which was characterized as [Fe^{III}Cp*(η^2-dtc)(THF)]$^+$BF$_4^-$, $\mathbf{4}^+\mathbf{BF_4}^-$, by comparison with an authentic sample prepared chemically in the CH_2Cl_2/THF solvent mixture.

The oxidation of **1** by [FeCp$_2$]$^+$PF$_6^-$, which is supposed to be even more endergonic (two carbonyl groups coordinated to Fe^{II}), is also driven by the follow-up chemistry of $\mathbf{2}^+\mathbf{PF_6}^-$, namely precipitation or ligand substitution, depending on working conditions. The thermodynamic potential of the $\mathbf{1}/\mathbf{1}^+$-$\mathbf{PF_6}^-$ system is unknown since the electrochemical oxidation is totally irreversible, even at scan rates as high as 5000 V s^{-1}, which is indicative of the extremely short lifetime of the 17e cation $\mathbf{1}^+$.[10a,20] However, the conversion of **1** to $\mathbf{2}^+\mathbf{X}^-$ proceeds at $E_{pa} = 1.25$ V vs. SCE at 20 V s^{-1}, and the $E°$ value of the closely related system $\mathbf{2}/\mathbf{2}^+\mathbf{X}^-$ is known. If one assumes that the replacement of CO by the free sulfur of the dtc ligand displaces $E°$ by about 1 V, $E°$ ($\mathbf{1}/\mathbf{1}^+\mathbf{X}^-$) should be approximately +1.65 V vs. SCE. Thus, the oxidation of **1** to $\mathbf{1}^+\mathbf{X}^-$ by [FeCp$_2$]$^+$X$^-$ is disfavored by 1.2 V (28 kcal/mol). It is driven by the extremely fast chelation of $\mathbf{1}^+\mathbf{X}^-$, by CO evolution, and by the precipitation of $\mathbf{2}^+\mathbf{X}^-$, since the yields of the crude complex $\mathbf{2}^+\mathbf{X}^-$ are virtually quantitative (X$^-$ = PF$_6^-$ or BF$_4^-$). Indeed, a study of the evolution of the respective yields of **2** and $\mathbf{2}^+\mathbf{PF_6}^-$ in the ETC (electron transfer chain) transformation of **1** into **2** as a function of the amount of catalyst [FeCp$_2$]$^+$PF$_6^-$ shows (Figure 1) that this electrocatalytic system is rapidly disrupted when the amount of the initiator is increased. The side reaction is the precipitation of $\mathbf{2}^+\mathbf{PF_6}^-$ in THF (the amount of precipitated $\mathbf{2}^+\mathbf{PF_6}^-$ is linearly proportional to the added quantities of the ferrocenium salt).

(20) (a) Fawcett, J. P.; Jackson, R. A.; Poë, A. J. *J. Chem. Soc., Chem. Commun.* **1975**, 733. (b) Fox, A.; Malito, J.; Poë, A. J. *J. Chem. Soc., Chem. Commun.* **1981**, 1052. (c) Poë, A. J. *Transition Met. Chem.* **1982**, *7*, 65. (d) Herrinton, T. R.; Brown, T. L. *J. Am. Chem. Soc.* **1985**, *107*, 5788. (e) McCulleen, S. B.; Walker, H. W.; Brown, T. L. *J. Am. Chem. Soc.* **1982**, *104*, 4007. (f) Shi, Q.-Z.; Richmond, T. G.; Trogler, W. C.; Basolo, F. *J. Am. Chem. Soc.* **1982**, *104*, 4032; **1984**, *106*, 71. (g) Trogler, W. C. *Int. J. Chem. Kinet.* **1987**, *19*, 1025. (h) Therien, M. J.; Ni, C.-L.; Anson, F. C.; Osteryoung, J. G.; Trogler, W. C. *J. Am. Chem. Soc.* **1986**, *108*, 4037. (i) Zizelman, P. M.; Amatore, C.; Kochi, J. K. *J. Am. Chem. Soc.* **1984**, *106*, 3771.

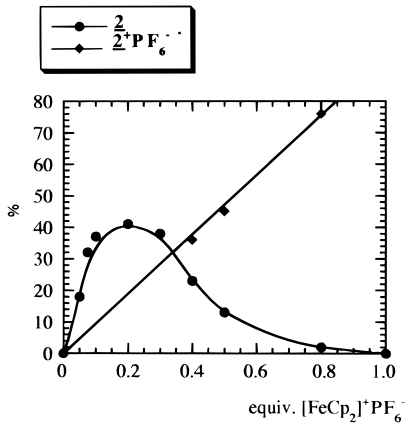

Figure 1. Evolution of the yields of **2** and $\mathbf{2}^+\mathbf{PF_6}^-$ during the electron-transfer-chain catalysis between **1** and [FeCp$_2$]$^+$PF$_6^-$.

Back reduction of the 17e complexes $\mathbf{2}^+\mathbf{PF_6}^-$ and $\mathbf{7}^+\mathbf{PF_6}^-$ using Na/Hg gives very unsatisfactory results, due to the affinity of Hg for sulfur, but the use of [Fe^{I}Cp(C$_6$Me$_6$)] is very convenient and 1e reduction using this reagent is very clean. It is noteworthy that replacement of the CO ligand in $\mathbf{2}/\mathbf{2}^+\mathbf{PF_6}^-$ by PPh$_3$ in $\mathbf{7}/\mathbf{7}^+\mathbf{PF_6}^-$ displaces the redox potential by almost 1 V. However, the same Fe^{II} (Fe^{III}) complexes can be used for 1e reduction (oxidation) showing the generality of their application in redox synthesis. The 18/19e system $\mathbf{9}^+\mathbf{PF_6}^-/\mathbf{9}$ (*vide infra*) can be handled similarly using the Fe^I and Fe^{III} sandwich compounds for passing from one oxidation state to the other.

Substitution Lability of the 17e Complexes [Fe^{III}Cp*(η^2-dtc)(L)]$^+$PF$_6^-$ and Intermediacy of 19e States. Kinetic Instability of $\mathbf{2}^+\mathbf{PF_6}^-$ in Polar Solvents. The impossibility of dissolving $\mathbf{2}^+\mathbf{PF_6}^-$ in any solvent without rapid CO evolution is indicative of the reactivity of this 17e complex. Dissolution and color change from green to purple blue or orange (depending on the solvent) are concomitant with the disappearance of the CO stretches in the infrared spectra. Thus, the CO ligand is very labile and the complex $\mathbf{2}^+\mathbf{PF_6}^-$ is kinetically unstable in solution despite the fact it can be stored at ambient temperature for several months in the solid state. The rate of CO evolution varies from one solvent to another, increasing with the coordination ability of the incoming solvent (Scheme 2). This CO substitution reaction leading to the Fe^{III} centered-radicals [Fe^{III}Cp*(η^2-dtc)(L)]$^+$PF$_6^-$ was monitored by visible spectroscopy in CH_2Cl_2 at 25 °C, in CH_3COCH_3 at 5 °C, and CH_3CN at 5 °C.[10d] The influence of the coordination ability of the incoming ligand on the reaction is indicated by the straight lines obtained by plotting $\ln(A - A_\infty) = f(t)$, thus demonstrating pseudo-first-order kinetics. The half-reaction times vary appreciably with the nature of the incoming ligand (Figure 2).

The high rate of CO exchange with CH_3CN ($t_{1/2}$ = 5 min at 5 °C) and CH_3COCH_3 ($t_{1/2}$ = 13.5 min at 5 °C) in $\mathbf{2}^+\mathbf{PF_6}^-$ contrasts with its thermal stability. The pseudo-first-order kinetics of these ligand exchange reactions and the large rate dependence on the basicity of the incoming ligand are in agreement with an associative mechanism involving 19e species as intermediates or transition states.[20] The associative mechanism for CO exchange with other ligands in 17e complexes was first recognized and demonstrated by Poë[20a-c] for Re(CO)$_5^•$. Subsequently this mechanism has been shown to be valid for several other 17e complexes.[20d-j] It results from the very low kinetic barrier for the 17 ⇄ 19e interconversion[21] and from the fact that 19e species have energies very close to those of 17e species.[22]

Scheme 2

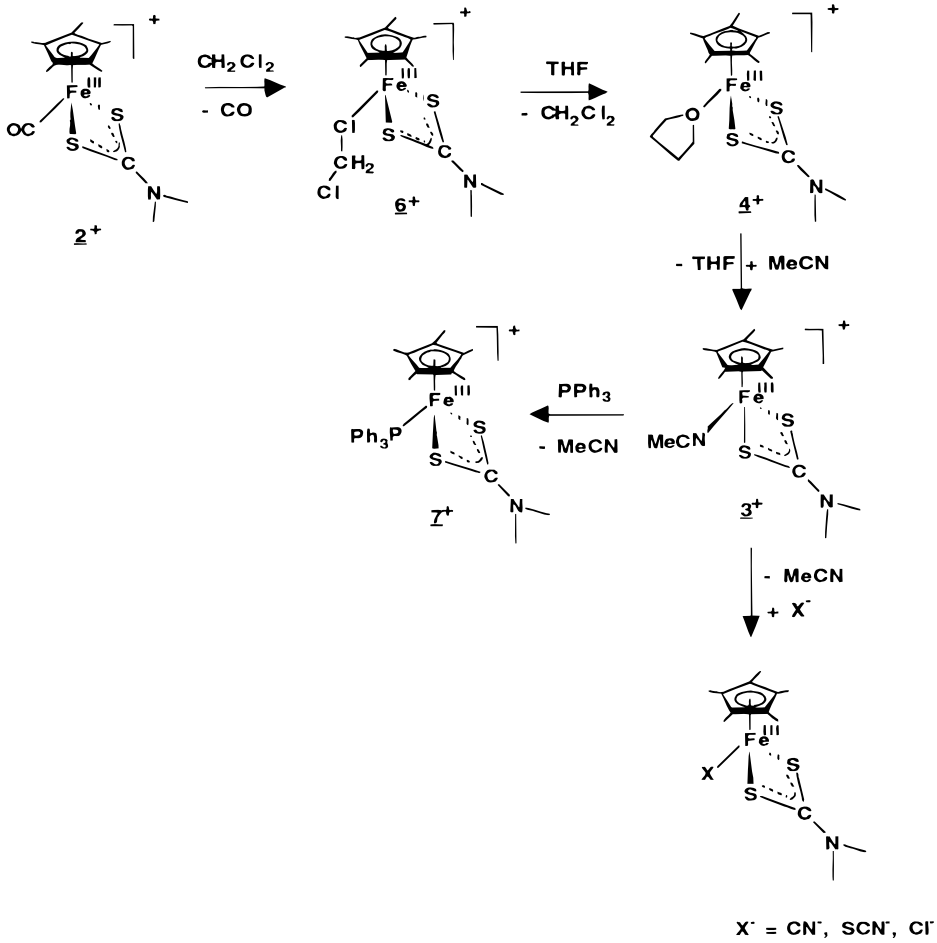

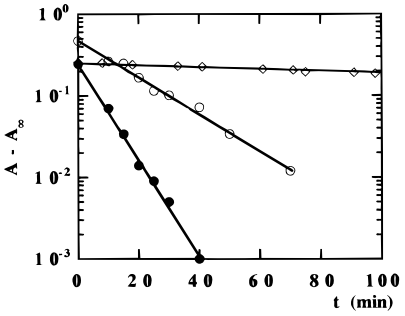

Figure 2. Evolution of the variation of absorbance with time ($\ln(A - A_\infty) = f(t)$) for the reaction of CO substitution in $\mathbf{2}^+\mathbf{PF_6}^-$ by a solvent molecule: ◇, in CH_2Cl_2 (25 °C); ○, in CH_3COCH_3 (5 °C); ●, in CH_3CN (5 °C). Semilogarithmic paper was used for the absorbance scale.

Reactivity of $\mathbf{2}^+\mathbf{PF_6}^-$ toward Neutral and Anionic Ligands. All these experiments convergently show the influence of both the ionic strength of the medium and the donor character of the incoming ligand on the ligand exchange. These weak 2e donor ligands in $\mathbf{2}^+\mathbf{PF_6}^-$–$\mathbf{6}^+\mathbf{PF_6}^-$ could easily be displaced by stronger ones; for instance, 2e phosphorus donors such as PPh_3 or $Ph_2PCH_2CH_2PPh_2$ produce $[Fe^{III}Cp^*(\eta^2\text{-dtc})(PPh_3)]^+PF_6^-$, $\mathbf{7}^+\mathbf{PF_6}^-$, and $[Fe^{III}Cp^*(\eta^2\text{-dtc})(\eta^1\text{-dppe})]^+PF_6^-$, $\mathbf{8}^+\mathbf{PF_6}^-$, respectively, while the anionic ligands such as CN^-, SCN^-, and Cl^- generate $[Fe^{III}Cp^*(\eta^2\text{-dtc})(CN)]$, **11**, $[Fe^{III}Cp^*(\eta^2\text{-dtc})(SCN)]$, **13**, and $[Fe^{III}Cp^*(\eta^2\text{-dtc})(Cl)]$, **14** (Scheme 2).

The simplest way of obtaining the complex $\mathbf{7}^+\mathbf{PF_6}^-$ involves the reaction of $\mathbf{2}^+\mathbf{PF_6}^-$ with 1 equiv of triphenylphosphine in acetone or acetonitrile. It can be obtained as well starting from **1** or **2**, ferrocenium hexafluorophosphate, and the desired phosphorus ligand in acetone or dichloromethane. Whereas $\mathbf{7}^+\mathbf{PF_6}^-$ is robust, the complex $\mathbf{8}^+\mathbf{PF_6}^-$ is rather labile and must be handled rapidly (see the characterization in Table 1). As in the case of $\mathbf{2}^+\mathbf{PF_6}^-$, $\mathbf{7}^+\mathbf{PF_6}^-$ can be reduced back to its neutral form **7** in good yield using 1 equiv of $[Fe^ICp(C_6Me_6)]$. The oxidation of the latter is completed with 1 equiv of ferrocenium hexafluorophosphate (Scheme 3).

Physical Properties of the 17e Fe^{III} Complexes. The main physical characterizations of the different complexes are given in Table 1 (see Experimental Section for others). The ESR parameters of all compounds show anisotropic *g* values characteristic of low-spin Fe^{III} complexes. The Mössbauer parameters isomer-shift (IS) and quadrupole splitting (QS) values, are typical for Fe–dtc complexes.[18,24]

The details of the X-ray crystal structure studies of **11** are summarized in Table 2, and significant bond distances and angles are given in Tables 3 and 4, respectively. The Fe–S distances are identical and close to those found in known complexes.[8,13,27] The S–C distances and the very short CN bond length (1.28 Å) are indicative of the η^2 coordination mode of the dtc ligand and the large contribution of the resonance

(21) Philbin, C. E.; Granatir, C. A.; Tyler, D. R. *Inorg. Chem.* **1986**, *25*, 4806.

(22) (a) Astruc, D. *Chem. Rev.* **1988**, *88*, 1189. (b) Ruiz, J.; Lacoste, M.; Astruc, D. *J. Chem. Soc., Chem. Commun.* **1989**, 813. (c) Ruiz, J.; Lacoste, M.; Astruc, D. *J. Am. Chem. Soc.* **1990**, *112*, 5471.

(23) Köelle, U.; Grätzel, M. *Inorg. Chem.* **1986**, *25*, 2689.

(24) (a) Burger, K.; Korecz, L.; Mag, P.; Belluco, U.; busetto, L. *Inorg. Chim. Acta* **1971**, *5*, 362. (b) Bancroft, G. N.; Butler, K. D.; Manzer, L. E.; Shaver, A.; Ward, J. H. *Can. J. Chem.* **1974**, *52*, 782. (c) Long, G. J.; Alway, D. G.; Barnett, K. W. *Inorg. Chem.* **1978**, *17*, 488.

(25) Bard, A. J.; Faulkner, L. R. *Electrochemical Methods*; Wiley: New York, 1980; Chapter 6.

(26) Wenger, P. E. *Analyse Quantitative Minérale*; Dunod: Paris, 1955; p 163.

Table 1. ESR and Mössbauer Data for Paramagnetic 17e (**2**$^+$−**8**$^+$ and **10**$^+$) and 19e (**9**) Fe^{III} and Diamagnetic Fe^{IV} Complexes

	ESR[a]			Mössbauer	
	g_1	g_2	g_3	IS[c]	QS[d]
[FeCp(η^1-dtc)(CO)$_2$]				−0.148	1.688
[FeCp(η^2-dtc)(CO)]				0.027	1.827
[FeCp*(η^2-dtc)(CO)]				0.210	1.940
[FeCp*(η^2-dtc)(PPh$_3$)], **7**				0.524	2.188
[FeCp*(η^2-dtc)(THF)]$^+$, **4**$^+$	2.323	2.050	2.004		
[FeCp*(η^2-dtc)((CH$_3$)$_2$CO)]$^+$, **5**$^+$	2.453	2.035	1.995		
[FeCp*(η^2-dtc)(CH$_2$Cl$_2$)]$^+$, **6**$^+$ [b]	2.571	2.135	1.990		
[FeCp*(η^2-dtc)(NCMe)]$^+$, **3**$^+$	2.672	2.007		0.550	0.620
	2.611[b]	2.188[b]	2.001[b]		
[FeCp*(η^2-dtc)(PPh$_3$)]$^+$, **7**$^+$	2.476	2.238	1.960	0.470	0.659
[FeCp*(η^2-dtc*)(PPh$_3$)]$^+$, **10**$^+$	2.666	2.004	1.941	0.462	0.631
[FeCp*(η^2-dtc)(η^1-dppe)]$^+$, **8**$^+$	2.636	2.157	1.975	0.445	0.665
[FeCp*(η^2-dtc)(CO)]$^+$, **2**$^+$	2.237	2.107	2.049	0.418	0.686
[FeCp*(η^2-dtc)$_2$]$^+$, **9**$^+$				0.460	0.220
[FeCp*(η^2-dtc)$_2$], **9**	2.275	2.029		0.540	0.940[e]
[FeCp*(η^2-dtc)(η^1-dtc)], **9′**	2.268	2.126	2.035	0.499	0.332
[FeCp*(η^2-dtc)(CN)], **11**	2.372	2.268	1.973	0.395	0.884
				0.330[e]	0.660[e]
[FeCp*(η^2-dtc**)(CO)]$^+$, **12**$^+$ [f]	2.322	2.055	1.999		
[FeCp*(η^2-dtc)(SCN)], **13**	2.483	2.088	1.997	0.460	0.660
				0.389[e]	0.587[e]
[Fe^{I}Cp(η^6-C$_6$Me$_6$)] (19e)[41]	2.063	2.000	1.864	0.850	0.560[g]
				0.850	1.180[g]
[Fe^I(C$_6$Me$_6$)$_2$]$^+$ [h] (19e)[16,41,42]	2.086	1.996	1.865	0.910	1.700[h]
[Fe^I(η^5-C$_6$Me$_6$H)(η^6-C$_6$Me$_6$)] (19e)[44,45]	2.144	2.0176	1.996	0.580	1.040
[Fe^{III}Cp*{(POMe)$_3$}$_2$(CH$_3$)]$^+$ (17e)[43]	2.352	2.045	1.997	0.550	0.600
[Fe^{III}Cp*(dppe)(CH$_3$)]$^+$ (17e)[43]	2.453	2.045	1.993		
[Fe^{I}Cp(η^1-dppe)(CO)] (17e)[46]	2.430	2.050	1.980		

[a] Solid-state sample (10 K) except when specified. [b] Frozen solution (20 K). [c] mm s^{-1} vs Fe at RT (77 K). [d] mm s^{-1} (77 K). PF_6^- was used as counteranion (dtc = S_2CNMe_2; dtc* = S_2CNEt_2). [e] Room temperature. [f] dtc** = $S_2CN(CH_2(C_6H_5))_2$.

Scheme 3

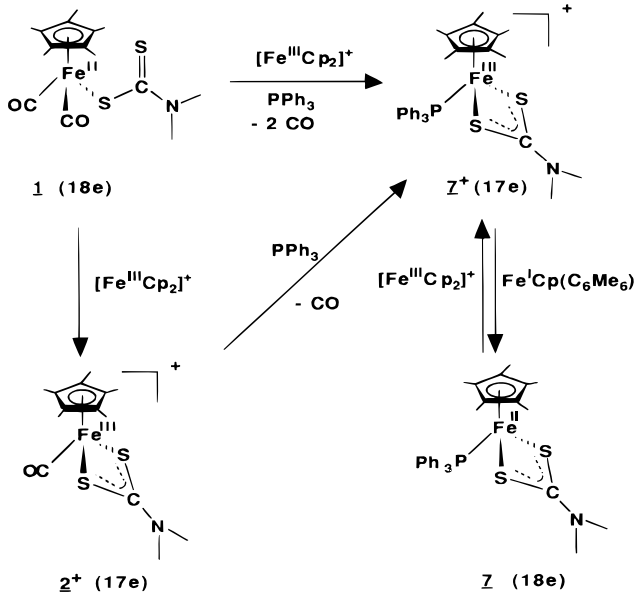

form II to the structure with a considerable CN double-bond character (confirmed by IR spectroscopy). In limiting form I, a sulfur electron pair is delocalized within the metal−chelate ring. On the other hand, in limiting form II, the nitrogen lone pair has been donated to the C−N bond. This locates a formal positive charge on the nitrogen atom and corresponds to a net shift of electron density on the sulfur atoms which are now less able to accept electron density from the iron.

form I form II

Oxidation of [Fe^{III}Cp*(η^2-dtc)(L)]$^+$PF$_6^-$ to [Fe^{IV}Cp*(η^2-dtc)$_2$]$^+$PF$_6^-$. The substitution lability of the 2e ligand in the complexes **2**$^+$**PF$_6^-$**−**8**$^+$**PF$_6^-$** can be extended to anionic ligands as shown above, but depending on the ligand, the 19e intermediates obtained can be very electron rich and act as reducing agents. Thus, the complexes **2**$^+$**PF$_6^-$**−**8**$^+$**PF$_6^-$** react with Na$^+$dtc$^-$·2H$_2$O (eq 3) to give the new complex [Fe^{IV}Cp*-

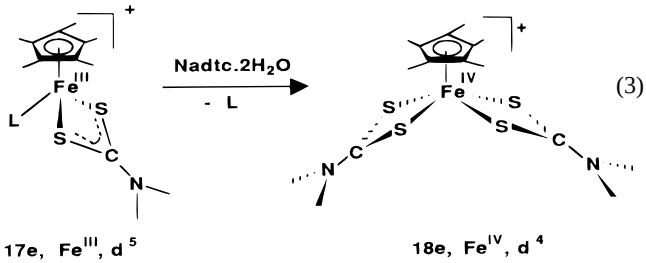

(3)

(η^2-dtc)$_2$]$^+$PF$_6^-$, **9**$^+$**PF$_6^-$** (75% yield), Na$^+$OH$^-$ (titrated by 0.01 N HCl), and H$_2$ (detected by gas chromatography). The reaction corresponds to the reduction of 1 mol of H$_2$O by the complex according to the following stoichiometry:

$$[Fe^{III}Cp^*(\eta^2\text{-dtc})(L)]^+PF_6^- + Na^+dtc^- + H_2O \rightarrow [Fe^{IV}Cp^*(\eta^2\text{-dtc})_2]^+PF_6^- + Na^+OH^- + {}^1/_2H_2 + L \quad (4)$$

Complex **9**$^+$**PF$_6^-$** can also be formed upon contact of an organic

(27) (a) Asirvatham, V. S.; Yao, Z.; Klabunde, K. J. *J. Am. Chem. Soc.* **1994**, *116*, 5493 and references therein. (b) Collins, T. J.; Fox, B. G.; H, Z. G.; Kostka, L.; Münck, E.; Rickard, C. E. F.; Wright, L. J. *J. Am. Chem. Soc.* **1992**, *114*, 8724. (c) Pasek, E. A.; Straub, D. K. *Inorg. Chem.* **1972**, *11*, 259. (d) Sellmann, D.; Geck, M.; Knoch, F.; Ritter, G.; Dengler, J. *J. Am. Chem. Soc.* **1991**, *113*, 3819. (e) Bakshi, E. N.; Delfs, C. D.; Murray, K. S.; Peters, B.; Homborg, H. *Inorg. Chem.* **1988**, *27*, 4318. (f) Martin, R. L.; Rohde, N. M.; Robertson, G. B.; Taylor, D. *J. Am. Chem. Soc.* **1974**, *96*, 3647.

Table 2. Crystallographic Data (Graphite-Monochromatized Mo Kα Radiation, $\lambda = 0.710\ 13$ Å) for the X-ray Structure Determinations of **11** and $\mathbf{16}^{+}\mathbf{PF_6}^{-}$

	11	$\mathbf{16}^{+}\mathbf{PF_6}^{-}$
formula	$C_{14}H_{21}N_2S_2Fe$	$C_{46}H_{47}F_6N_2S_4PFe$
mol wt	337.30	956.92
cryst size, mm^3	0.20 × 0.13 × 0.13	0.50 × 0.20 × 0.20
cryst syst	triclinic	monoclinic
space group	$P\bar{1}$	*C*2/*c*
cell dimens		
a, Å	8.637(2)[a]	18.639(3)
b, Å	9.087(2)	21.757(4)
c, Å	11.593(1)	24.283(5)
α, deg	94.95(3)	90
β, deg	91.06(3)	112.23(2)
	113.67(3)	90
γ, deg	828.8(3)	9115(6)
V, Å^3	2	8
Z	1.352	1.395
d_{calcd}, g cm^3	11.50	6.09
	1275	7640
μ(Mo Kα), cm^{-1}	1254	6895
no. of data collcd	297(1)	297(1)
no. of unique data used	175	585
temp, K	3.5−50	3−50
no. of params varied	SHELXA	SHELXA
2*θ* range, deg	0.9179/0.0637	0.9552/0.4706
abs corr	0.003(3)	none
max/min transm	0.0495	0.0385
ext coef, χ[b]	0.1262	0.0961
*R*1		
w*R*2		

[a] Numbers in parentheses are estimated standard deviations in the least significant digits. [b] $F^* = F[1 + 0.001\chi F^2\lambda^3/\sin(2\tau)]^{-1/4}$.

Table 3. Significant Interatomic Distances (Å) in Complex **11**[a]

Fe−Cp(centroid)	1.709(6)	Fe−C10	1.89(4)
Fe−S1	2.285(4)	S1−C6	1.687(13)
Fe−S2	2.241(4)	S2−C6	1.739(13)
Fe−C1	2.10(2)	N1−C6	1.28(2)
Fe−C2	2.07(2)	N1−C8	1.44(2)
Fe−C3	2.126(12)	N1−C9	1.49(2)
Fe−C4	2.13(3)	N2−C10	1.22(6)
Fe−C5	2.09(2)		

[a] Numbers in parentheses are estimated standard deviations in the least significant digits.

Table 4. Significant Intramolecular Angles (deg) in Complex **11**[a]

S1−Fe−S2	76.4(2)	C6−N1−C9	121.0(11)
S1−Fe−C10	95.6(9)	C8−N1−C9	118.6(12)
S2−Fe−C10	97.0(6)	Fe−C10−N2	175.(3)
Fe−S1−C6	86.8(5)	S1−C6−N1	125.1(9)
Fe−S2−C6	87.0(5)	S2−C6−N1	125.2(9)
C6−N1−C8	120.4(12)	S1−C6−S2	109.7(8)

[a] Numbers in parentheses are estimated standard deviations in the least significant digits.

solution of the 17e complexes $\mathbf{2}^{+}\mathbf{PF_6}^{-}$−$\mathbf{8}^{+}\mathbf{PF_6}^{-}$ with a slight excess of water. Clearly, the second dtc ligand must come from decomposition of another molecule of $\mathbf{2}^{+}\mathbf{PF_6}^{-}$−$\mathbf{8}^{+}\mathbf{PF_6}^{-}$ and, as expected, the yields are lower (30−40%) than if the dtc ligand is added. Workup of the reaction mixtures results in the isolation of inorganic Fe^{III} hydroxide as well as pentamethylcyclopentadiene.

The intermediacy of complex $[Fe^{III}Cp^*(dtc)_2]$ in the mechanism of conversion of $\mathbf{2}^{+}\mathbf{PF_6}^{-}$ to $\mathbf{9}^{+}\mathbf{PF_6}^{-}$ (eq 4) is indicated by the reduction of H_2O. Water is present in the reaction as a dihydrate in $Na^+dtc^-\cdot 2H_2O$ and serves as an acceptor to trap the 19e species **9** or **15**. Since the conversion **15** ⇄ **9** at the 19e level is expected to be very fast as compared to water reduction, we propose that reduction of water is effected by **9** and not by **15**. Considering that the anionic dtc ligand is a much stronger nucleophile than the neutral water molecule and that Fe is not very oxophilic, the first step involves the attack of dtc on $\mathbf{2}^{+}\mathbf{PF_6}^{-}$ (or $\mathbf{3}^{+}\mathbf{PF_6}^{-}$−$\mathbf{8}^{+}\mathbf{PF_6}^{-}$) which must be fast when L is a weak ligand ($\mathbf{2}^{+}\mathbf{PF_6}^{-}$−$\mathbf{6}^{+}\mathbf{PF_6}^{-}$) and slow with bulky ligands such as PPh_3 ($\mathbf{7}^{+}\mathbf{PF_6}^{-}$) or dppe ($\mathbf{8}^{+}\mathbf{PF_6}^{-}$). The overall mechanism is shown in eqs 5−8 (PF_6^- as counteranion).

$$\underset{\mathbf{2}^{+}-\mathbf{8}^{+},\ 17e}{[FeCp^*(\eta^2\text{-dtc})(L)]^+} + dtc \rightarrow \underset{\mathbf{15},\ 19e}{[FeCp^*(\eta^2\text{-dtc})(\eta^1\text{-dtc})(L)]} \quad (5)$$

$$\underset{\mathbf{15},\ 19e}{[FeCp^*(\eta^2\text{-dtc})(\eta^1\text{-dtc})(L)]} \rightleftarrows \underset{\mathbf{9}',\ 17e}{[FeCp^*(\eta^2\text{-dtc})(\eta^1\text{-dtc})]} + L \quad (6)$$

$$\underset{\mathbf{9}',\ 17e}{[FeCp^*(\eta^2\text{-dtc})(\eta^1\text{-dtc})]} \rightarrow \underset{\mathbf{9},\ 19e}{[FeCp^*(\eta^2\text{-dtc})_2]} \quad (7)$$

$$\underset{\mathbf{9},\ 19e}{[FeCp^*(\eta^2\text{-dtc})_2]} + H_2O \rightarrow \underset{\mathbf{9}^{+},\ 18e}{[FeCp^*(\eta^2\text{-dtc})_2]^+} + Na^+OH^- + {}^1/_2H_2 \quad (8)$$

Considering the 17e ⇄ 19e equilibrium of eq 9 (*vide infra*), it is reasonable to assume that water reduction is achieved by the more electron-rich 19e chelate form **9**. Inner-sphere reduction via protonation of **9** could be envisaged by comparison with the known mechanism of reduction of water by the 19e complex $[CoCp_2]$.[23]

Crystal Structure of the Fe^{IV} Complex. The details of the X-ray crystal structure studies of $\mathbf{16}^{+}\mathbf{PF_6}^{-}$ are summarized in Table 2, and significant bond distances and angles are given in Tables 5 and 6, respectively. Complex $\mathbf{16}^{+}\mathbf{PF_6}^{-}$was synthesized

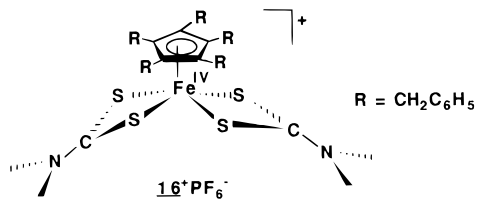

in order to obtain a crystal structure of the first $C_5R_5Fe^{IV}$

Table 5. Significant Interatomic Distances (Å) in Complex $\mathbf{16}^{+}\mathbf{PF_6}^{-}$[a]

Fe−Cp(centroid)	1.799(2)	Fe−C10	2.190(4)
Fe−S1	2.329(2)	Fe−C11	2.117(4)
Fe−S2	2.318(2)	S1−C1	1.694(5)
Fe−S3	2.334(2)	S2−C1	1.693(5)
Fe−S4	2.318(2)	S3−C4	1.710(5)
Fe−C7	2.124(4)	S4−C4	1.685(5)
Fe−C8	2.186(4)	N1−C1	1.309(6)
Fe−C9	2.221(4)	N2−C4	1.302(6)

[a] Numbers in parentheses are estimated standard deviations in the least significant digits.

Table 6. Significant Intramolecular Angles (deg) in Complex $\mathbf{16}^{+}\mathbf{PF_6}^{-}$[a]

S1−Fe−S2	71.95(6)	S1−C1−S2	107.4(3)
S1−Fe−S3	122.45(6)	S3−C4−S4	107.6(3)
S2−Fe−S4	119.34(6)	N1−C1−S1	125.6(4)
S3−Fe−S4	72.19(5)	N1−C1−S2	127.0(4)
C1−S1−Fe	90.1(2)	N2−C4−S3	125.5(4)
C1−S2−Fe	90.5(2)	N2−C4−S4	126.8(4)
C4−S3−Fe	89.4(2)	C2−N1−C3	118.6(5)
C4−s4−Fe	90.6(2)	C5−N2−C6	116.7(5)

[a] Numbers in parentheses are estimated standard deviations in the least significant digits.

Scheme 4

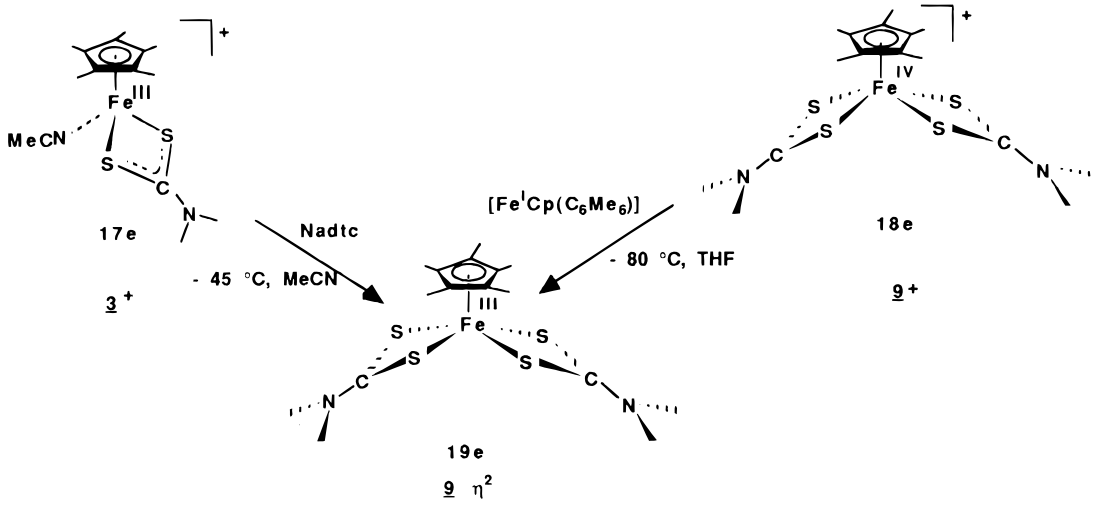

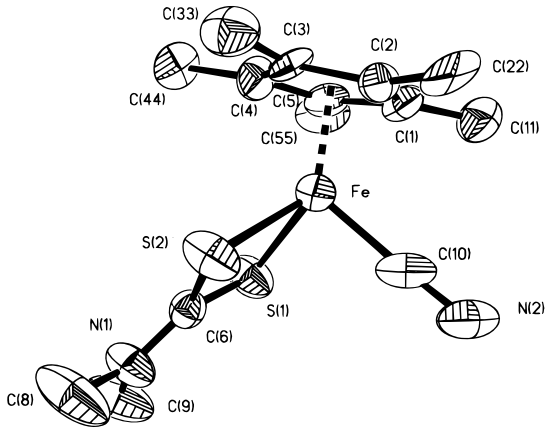

Figure 3. ORTEP view of the X-ray structure of the 17e complex **11**.

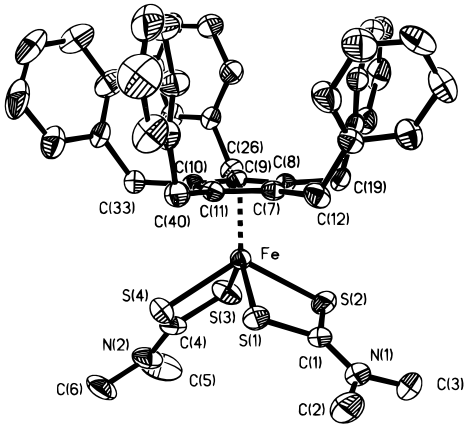

Figure 4. ORTEP view of the X-ray structure of complex **16**$^+$**PF$_6$**$^-$.

organometallic complex (R ≠ Me). Several different attempts were made to obtain good-quality crystals of **9**$^+$**PF$_6$**$^-$. Even though these attempts were apparently successful, these samples underwent a slow degradation during data collection and only allowed the determination of basic parameters (this complex crystallizes in a monoclinic system: $a = 12.27$, $b = 17.51$, $c = 13.15$ Å; $\beta = 90.6°$; $V = 2826$ Å^3; $Z = 4$; $d = 1.40$ g/cm^3). However, use of the pentabenzylcyclopentadienyl ligand (Cp**)[39] permitted the acquisition of a satisfactory X-ray crystal structure.

Examination of the different metrical parameters of **16**$^+$**PF$_6$**$^-$ shows that it follows the same trends as those of **11** and other Fe^{III} or Fe^{IV} dithiocarbamate complexes (Figures 3 and 4).[8,13,27] The Fe−S, S−C, and C−N bond distances for complex

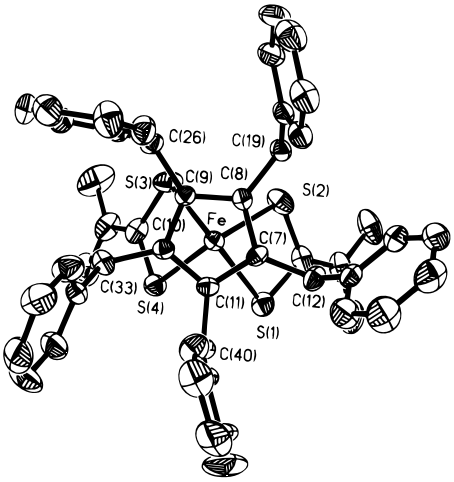

Figure 5. On top ORTEP view of **16**$^+$**PF$_6$**$^-$ showing the clockwise directionality of the benzyl groups.

16$^+$**PF$_6$**$^-$ are very close to the values reported for other Fe^{IV} complexes regardless of the spin configuration of the metal.[27] These data confirm the important contribution of form II to the electronic structure. The four Fe−S distances are identical within experimental error and are short enough to be sure of the electron density between the two atoms. Unlike in other piano-stool Cp** complexes,[39] all five benzyl groups are directed away from the metal center and the benzylic carbons are all slightly above the mean Cp plane. This is undoubtedly due to the large steric effect of both dtc ligands. The orientation of the phenyl groups is clockwise as illustrated in Figure 5. The bond lengths for the Cp** ring are almost identical (ca. 1.42 Å) and close to the values reported for other Cp** complexes.[39] The Fe−Cp centroid distance is 1.799 Å. The bond angles in the Cp** ring do not deviate from 108°, and consequently, the ring is essentially planar even though it is tilted by 3.5° from the normal plane.

17e and 19e States of Complex [Fe^{III}Cp*(dtc)$_2$]. Spectroscopic Data. The 19e complex [Fe^{III}Cp*(η^2-dtc)$_2$] can be synthesized either by addition of anhydrous Na$^+$dtc$^-$ to a 17e solvent complex [Fe^{III}Cp*(η^2-dtc)(solvent)]$^+$ such as **3**$^+$**PF$_6$**$^-$ at −45 °C in CH_3CN solution or by one-electron reduction of the 18e cation [Fe^{IV}Cp*(η^2-dtc)$_2$]$^+$PF$_6^-$ using [Fe^{I}Cp(C$_6$Me$_6$)] as reducing reagent in THF solution at −80 °C (Scheme 4).

Both reactions afford a blue solution whose ESR spectrum at 20 K in the solid state exhibits axial symmetry with two g values ($g_\perp = 2.275$, $g_\parallel = 2.029$). This spectrum (Figure 6) is

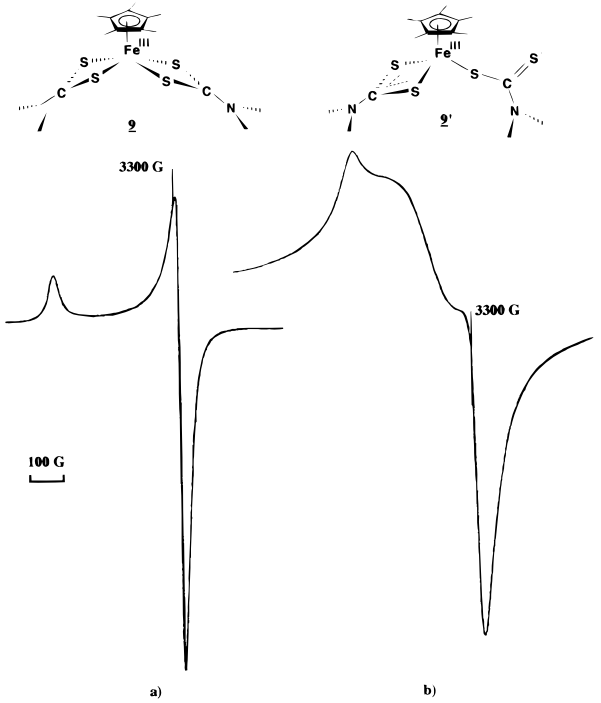

Figure 6. ESR spectra of **9** and **9′** at 20 K (solid-state sample).

indicative of a metal-based radical and contrasts with the rhombic distortion characterized by three *g* values which are recorded for all the 17e complexes $\mathbf{2}^{+}-\mathbf{13}$. When the solvent is removed from this blue solution at −35 °C, a blue microcrystalline powder can be isolated. Transfer to the Mössbauer cell in the drylab leads to the observation of a Mössbauer quadrupole doublet with IS = 0.54 mm s^{-1} vs. Fe and QS = 0.94 mm s^{-1} at 77 K (Figure 7a and Table 1). These parameters are markedly different from those of the 17e family. Whereas **9** has been shown to be thermally stable for up to 2 weeks in the solid state, it decomposes in MeCN solution above −40 °C to give a purple complex whose ESR spectrum exhibits the characteristic three *g* values of the 17e family (see Table 1 and Figure 6): $g_1 = 2.268$, $g_2 = 2.126$, $g_3 = 2.035$.

The Mössbauer spectrum of **9** in the solid state at room temperature also shows the disappearance of the doublet of the 19e complex and growth of a new doublet whose parameters correspond to those of the 17e family (see Table 1 and Figure 7c). The 19e complex is more stable (a) in nonpolar solvents and (b) when it is separated from the $Na^{+}PF_6^{-}$ salt which formed during the synthesis. For instance, extraction of this complex with toluene at −80 °C leads to a solution of the 19e form which is stable for several hours at this temperature. The $\{^1H\}^{13}C$ NMR spectra of both the 17e and 19e forms were obtained. The symmetrical 19e complex, **9**, exhibits three peaks at 59.71, 30.37, and 11.22 in d^8-toluene solution (298 K) and 68.41, 26.34, and 9.93 ppm in CD_3CN solution vs. $SiMe_4$ (253 K, 273 K) for C_{quat} (Cp*), N*Me*$_2$, and C_5*Me*$_5$ respectively. For the 17e form, both the mono- and bidentate dtc ligands were observed: 68.91 (C_{quat} (Cp*)), 38.52 and 31.20 (N*Me*$_2$), and 9.93 (C_5*Me*$_5$) in CD_3CN (253 or 273 K). In addition, satisfactory elemental analysis was obtained. It is striking, however, that the stability of both the 17e and 19e species is much lower in a polar solvent such as MeCN which is also a good ligand. In this solvent, neither the 17e nor the 19e form is stable at room temperature, which necessitates a more complete investigation of their interconversion in this solvent. However, if it is assumed that the ^{13}C relaxation times are similar for both species, the ^{13}C NMR spectrum shows a proportion of 19e/17e complexes of 0.5 at 253 K, which is indicative of the following thermodynamic equilibrium at this temperature:

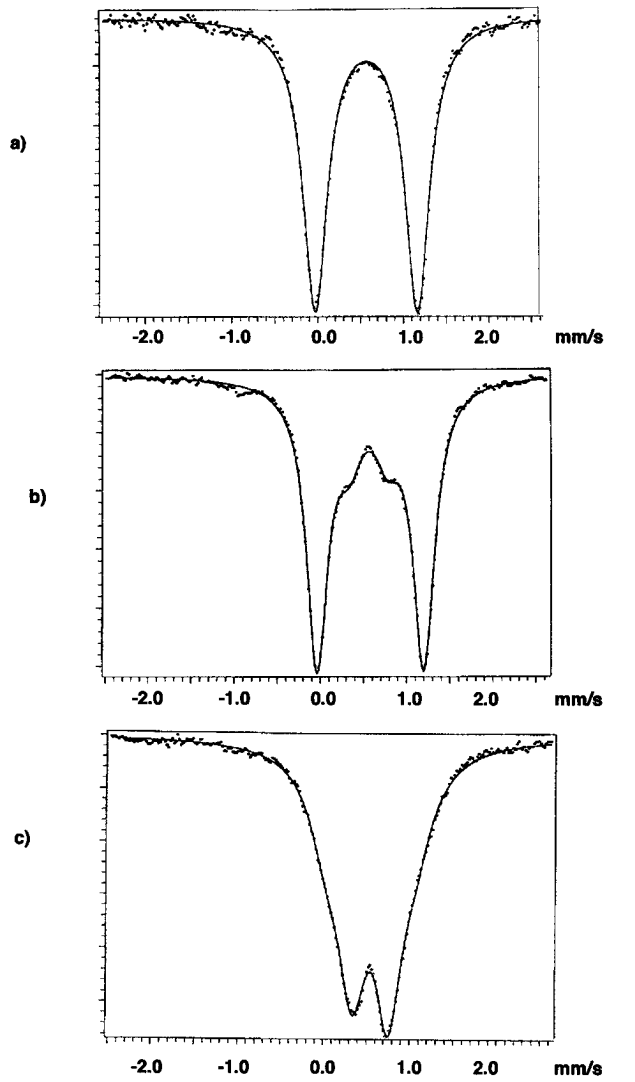

Figure 7. Iron-57 Mössbauer spectra of **9** recorded at 77 K showing the transformation of complex **9** to **9′** with time: (a) fresh sample; (b) after 6 days at 300 K; (c) after 26 days at 300 K.

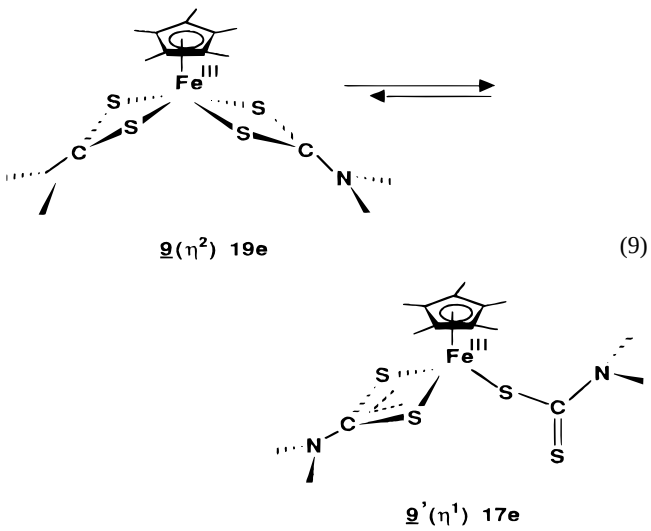

(9)

The absence of signals for coordinated MeCN means that either the 19e species [FeCp*(η^2-dtc)(η^1-dtc)(NCMe)] is not present in a detectable amount or that its interconversion with the 17e species is faster than the NMR time scale. The 19e form is

Chart 1

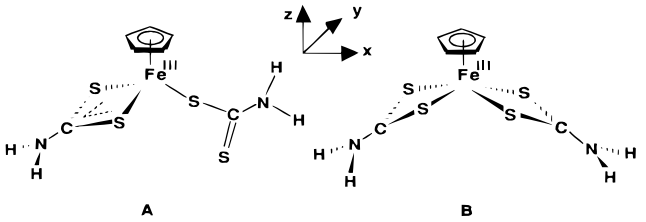

stabilized by the entropy effect of the dtc ligand, although it is a pseudoheptacoordinate complex. The 17e form is itself stabilized by pseudohexacoordination. It seems that both the 17e and 19e states are relatively stable in nonpolar solvents and in the solid state in contrast to the behavior in MeCN in the presence of $Na^+PF_6^-$ salt. A reasonable explanation for this observation is the salt-induced disproportionation of the radicals, an effect already documented for other organometallic radicals. The mechanism of the salt-induced disproportionation involves double ion-pair exchange driving the dismutation electron transfer reaction.[22]

Theoretical Study. In order to provide a better insight into the electronic factors governing the equilibrium represented in eq 9, we have carried out MS−SCF−X_α calculations on the 17e and 19e models [CpFe(η^1-S$_2$CNH$_2$)(η^2-S$_2$CNH$_2$)] (**A**) and [CpFe(η^2-S$_2$CNH$_2$)$_2$] (**B**). This type of calculation provides reliable qualitative results. Thus, previous calculations on 19e iron complexes[28] have shown that they correctly reproduce the level ordering and occupation, as well as the energy gaps, which is not always the case for this type of electron-rich complex when modeled with simple extended-Hückel MO calculations.[29] The choices for the geometries of **A** and **B** (Chart 1), were based on the experimental structures of related 18e and 17e compounds (see the Experimental Section for the geometrical and computational details).

The problem of the relative stabilities of the 17e/19e states is directly related to the electronic structure of their parent 18e species. The MO diagram of a stable 18e complex generally exhibits a significant gap which separates its nonbonding (or bonding) HOMO from its antibonding LUMO. This gap confers stability on the complex. This stability is reduced if one supplementary electron is added, since this electron is forced to occupy an antibonding level. A simple way to cancel the antibonding nature of the singly occupied HOMO of this 19e system is via ligand dissociation. If one ligand is lost, an antibonding level becomes nonbonding, and the situation becomes that of a stable 18e system which has lost one electron. Apparently, this 17e state appears more favorable than the 19e one. However, it should be recognized that the effect of ligand loss is not only the stabilization of the odd electron but also the destabilization of two M−L σ-bonding electrons which become the nonbonding pair of the dissociated ligand. Consequently, the relative stability of the 17e/19e states is the result of a delicate balance between bonding and antibonding effects. This situation is somewhat related to the 3e bond problem,[30] although it has been shown that such a relationship is not always so straightforward.[31] The two isomers depicted in eq 9 belong to the d^5 CpML$_4$ and CpML$_3$ general types, respectively. The qualitative d-type level ordering and occupation of such complexes are shown schematically in Figure 8. A formally hexacoordinated CpML$_3$ system exhibits the usual splitting of three nonbonding levels below two antibonding ones,[32] with a hole in the nonbonding block. On the other hand, the formally heptacoordinated CpML$_4$ species presents the opposite splitting of two below three,[33] with one single electron located in the antibonding block. For each system, it is of course not possible to predict a priori which is the singly occupied level among the group of three nonbonding (17e) or antibonding (19e) levels. In addition, more complicated situations can arise from the peculiar nature of the ligands. For example, the 19e situation shown in Figure 8 can be different if one of the ligands possesses a low-lying antibonding orbital which is capable of full or partial delocalization of the odd electron away from the metal.[28a,30] This could, in fact, be the case for **9** with the π^* LUMO of the dtc ligand acting as an electron sink. Such a situation would correspond to a formally 18e Fe^{IV} metal with a reduced ligand system. On the other hand, the 17e MO diagram of Figure 8 can also be different if a ligand possesses some high-lying nonbonding lone pairs which can pass above the nonbonding d block. In such a case, the odd electron could be located in a ligand-based rather than in a metallic orbital. This might be the case of the 17e species reported here, owing to the rather high energy of a sulfur lone pair. Such a situation would formally correspond to an 18e Fe^{II} system with an electron deficiency on the ligand.

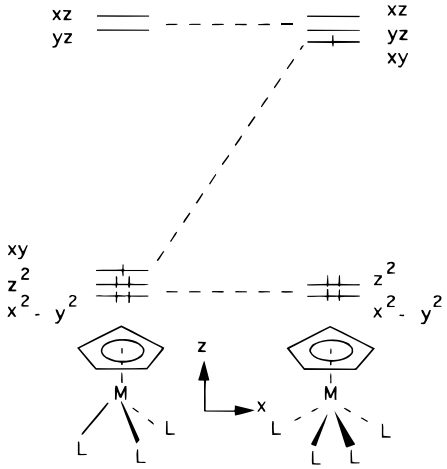

Figure 8. Qualitative d-type MO diagram of a 17e CpML$_3$ complex (left) and 19e CpML$_4$ complex (right).

The computed energies and charge distributions for the highest occupied and lowest unoccupied levels of **A** are listed

(28) (a) Lacoste, M.; Rabaâ, H.; Astruc, D.; Ardoin, N.; Varret, F.; Saillard, J.-Y.; Le Beuze, A. *J. Am. Chem. Soc*. **1990**, *112*, 9548. (b) Lacoste, M.; Rabaâ, H.; Astruc, D.; Ardoin, N.; Précigoux, C.; Saillard, J.-Y.; Le Beuze, A.; Courseille, C. *Organometallics* **1989**, *8*, 2233. (c) Rabaâ, H.; Chraibi, M.; Saillard, J.-Y.; Le Beuze, A.; Astruc, D. *J. Mol. Struct. (Theochem.)* **1991**, *251*, 57.

(29) As a matter of fact, standard extended-Hückel calculations on **B** lead to a wrong ground-state electronic configuration, with the odd electron located in a π^*(dtc) combination (unpublished results).

(30) Tyler, D. R. *Acc. Chem. Res*. **1991**, *24*, 325.

(31) Lin, Z.; Hall, M. B. *Inorg. Chem*. **1992**, *31*, 2791.

(32) Albright, T. A.; Burdett, J. K.; Whangbo, M. H. *Orbital Interactions In Chemistry*; Wiley-Interscience: New York, 1985.

(33) Kubacek, P.; Hoffmann, R.; Halvas, Z. *Organometallics* **1982**, *1*, 180.

(34) At the suggestion of a reviewer, we have explored the viability of this hypothesis experimentally. The reaction of *n*-Bu$_3$SnH with the purple 17-electron complex **9′** was carried out at −30 °C in THF solution and yielded a mixture of Cp*H, Me$_2$NC(S)H, and (Bu$_3$Sn)$_2$S. The most plausible origin of Cp*H is that it arises from the decomposition of [FeCp*(dtc)H] which, in turn, is formed via hydrogen atom abstraction from *n*-Bu$_3$SnH by the radical iron center. On the other hand, Me$_2$NC(S)H and (*n*-Bu$_3$Sn)$_2$S are probably formed by attack of *n*-Bu$_3$SnH or *n*-Bu$_3$Sn at the S−C bond of the dtc ligand. By means of independent experiments, it was established that these compounds are not formed by the reaction of *n*-Bu$_3$SnH with diamagnetic sources of dithiobarbamate. We therefore conclude that the observed reactivity pattern is in accord with the theoretical and spectroscopic arguments and that collectively these results imply that the spin density is delocalized on both the iron and the sulfur atoms. However, we also know that organometallic radicals can react with the part of the molecule that possesses the lowest ground-state spin density.[22a]

Table 7. Energy and Charge Distribution of the Highest Occupied and Lowest Unoccupied One-Electron Levels of [CpFe(η^1-S_2CNH_2)(η^2-S_2CNH_2)] (**A**)

			charge distribn (%)				
level	occ	E (eV)	Fe	Cp	η^1-dtc[a]	η^2-dtc[a]	[I + O][b]
18a″	0	−3.08	01	00	56	14	29
26a′	0	−4.50	02	00	01	66	31
25a′	0	−5.03	53	14	12	06	15
17a″	0	−5.02	54	14	00	18	15
24a′	1	−6.70	17	01	44	13	25
16a″	2	−6.88	40	03	28	10	19
15a″	2	−7.24	60	08	07	13	12
14a″	2	−7.31	09	02	48	15	26
23a′	2	−7.34	55	01	20	07	17
13a″	2	−7.89	07	02	22	39	30
22a′	2	−8.35	25	06	25	22	22
12a″	2	−8.55	15	07	38	11	29

[a] dtc = S_2CNH_2. [b] I = intersphere region (always < 2%); O = outer−sphere extramolecular region.

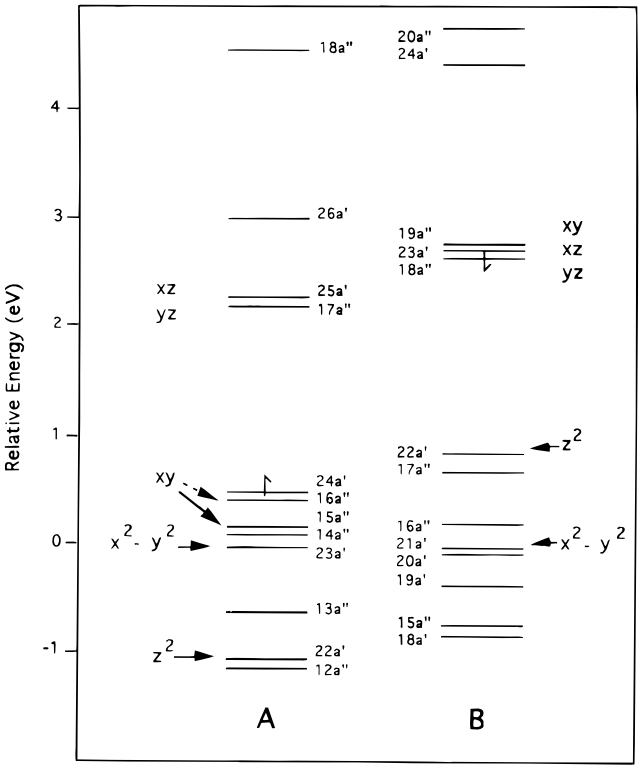

Figure 9. MO diagram of 17e and 19e models [CpFe(η^1-S_2CNH_2)(η^2-S_2CNH_2)] (**A**) and [CpFe(η^2-S_2CNH_2)$_2$] (**B**). They have been rescaled by placing their essencially nonbonding x^2-y^2 levels at the same energy.

in Table 7. The MO diagram for **A** is shown on the left-hand side of Figure 9. Although the expected three-below-two splitting of the d-type orbitals is observed, the nonbonding metal and sulfur blocks are overlapping in such a way that some mixing between them occurs. The HOMO 24a′ is a ligand orbital which is preponderantly located on the uncoordinated sulfur atom (41%). The next occupied MO (16a″) is more metal-centered, but it also possesses some sulfur character (14% on each sulfur of the monodentate dtc). The 24a′ and 16a″ orbitals are plotted in Figure 10. They are very close in energy. The ground-state configuration is computed to be $(16a'')^2(24a')^1$, 0.30 eV more stable than the $(24a')^2(16a'')^1$ configuration. Spin-polarized calculations lead to a similar value (0.35 eV), with a ground-state spin density of 60% on the uncoordinated sulfur atom. At level of accuracy of the present calculations, this energy difference lies at the limit of significance. We have checked that reasonable structural changes do not significantly

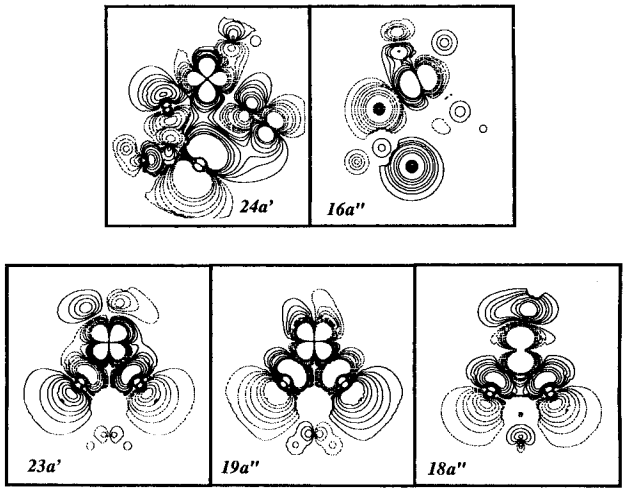

Figure 10. Plots of some frontier orbitals of **A** (top) and **B** (bottom): 24a′, in the *xz* plane; 16a″ in a plane parallel to *xz* and situated 0.5 au away from Fe; 23a′, 18a″, and 19a″, in Fe(η^2-dtc) plane.

Table 8. Energy and Charge Distribution of the Highest Occupied and Lowest Unoccupied One-Electron Levels of [CpFe(η^2-S_2CNH_2)$_2$] (**B**)

			charge distribn (%)			
level	occ	E (eV)	Fe	Cp	dtc[a]	[I + O][b]
20a″	0	−3.09	00	01	75	24
24a′	0	−3.36	00	10	50	40
19a″	0	−5.21	40	03	41	16
23a′	0	−5.30	51	18	17	15
18a″	1	−5.31	51	20	17	15
22a′	2	−7.05	65	02	21	12
17a″	2	−7.27	02	00	71	27
16a″	2	−7.66	00	06	68	26
21a′	2	−7.91	88	02	02	08
20a′	2	−8.04	04	04	61	31
19a′	2	−8.36	06	17	49	28
15a″	2	−8.92	24	01	50	25
18a′	2	−8.98	06	20	44	30

[a] dtc = S_2CNH_2. [b] I = intersphere region (always < 2%); O = outer−sphere extramolecular region.

modify this result. In particular, a variation of the Fe−S−C angle associated with the η^1-dtc ligand, from the assumed value of 120 to 113°, leads to the quasi-degeneracy of both configurations and results in a larger metallic character for the 16a″ level (44%). On the other hand, an increase of this bond angle tends to reinforce slightly the preference for the $(24a')^2(16a'')^1$ ground state. From these results, it can be concluded that some significant spin delocalization occurs on the ligands.

The energies and charge distributions for the highest occupied and lowest unoccupied levels of **B** are listed in Table 8. The MO diagram for **B** is shown on the right-hand side of Figure 9. As in the case of **A**, the nonbonding fully occupied metal and sulfur blocks are overlapping. On the other hand, the three antibonding d-type levels (18a″, 23a′, and 19a″, plotted in Figure 10) are fairly isolated (by 1.95 eV) with respect to the two lowest levels derived from the π^* dtc orbitals (24a′ and 20a″), thus indicating that the odd electron is forced to occupy a metallic orbital. In fact, the $(18a'')^1$ and $(23a')^1$ configurations are computed to be quasi-degenerate.[31] A way of stabilizing a π^* dtc orbital, and perhaps to render it occupied in **B**, is to rotate the NR_2 group by 90° around the CN axis. Since this orbital is somewhat C−N antibonding in the planar form, this antibonding character is lost when the CS_2 and NR_2 planes are perpendicular. The calculations were performed with the NH_2 groups of **B** oriented perpendicular to their corresponding CS_2 groups, thus maintaining the overall C_s symmetry. As a consequence, the

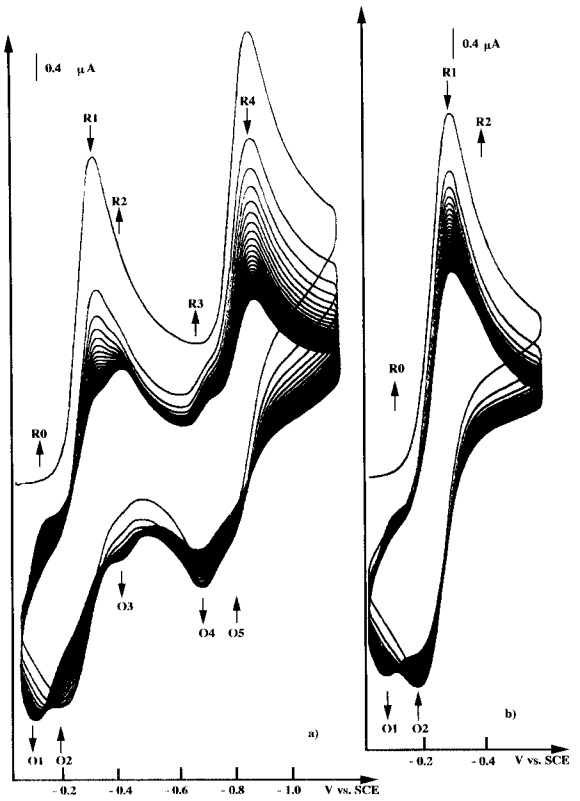

Figure 11. Cyclic voltammogram under continuous scan of 2.22 × 10^{-5} M **2**$^+$**PF$_6$**$^-$ in DMF solution (0.1 M ^{n}Bu$_4$NBF$_4$, at Pt electrode, scan rate = 0.6 V/s, 20 °C): (a) switching potential beyond the second electron transfer; (b) switching potential between both electron transfers.

π* dtc levels were found to be lower in energy but still of too high an energy to be occupied (0.66 eV above the antibonding d-block). On the basis of this result, one can conclude that **B** is a genuine Fe^{III} 19e complex, in full agreement with the experimental data.

Electrochemical Data. The voltammogram for **9**$^+$**PF$_6$**$^-$ provides additional information concerning both the neutral radical **9** and the anion **9**$^-$ generated by cathodic reduction, with particuler reference to the decoordination of a dtc ligand for these species on the electrochemical time scale. Although the CV looks somewhat complex at first sight, it is possible to obtain substantial information by continuous cycling. Two regions can be clearly distinguished: the left-hand side corresponds to redox interconversions between the cationic and the neutral species (derived from **9**$^{+/0}$), and the right-hand side relates to redox interconversions between the neutral and the anionic species (derived from **9**$^{0/-}$).

Figure 11a shows the entire CV, while Figure 11b represents the continuous scan of the left zone only (**9**$^{+/0}$) with a switching potential situated before the second reduction wave. The comparison of the two figures emphasizes the observation of the decoordination of one dtc ligand. In Figure 11b, the Nernstian wave corresponding to **9**$^{+/0}$ is clearly apparent (R1/O2). Upon continuous scan, the intensities of both the cathodic and anodic sides of the wave decrease, thus indicating that the couple **9**$^{+/0}$ slowly disappears from the proximity of the electrode. Concomitant with the disappearance of **9**$^{+/0}$, two waves increase upon continuous scanning: R0/O1 at a less negative potential than **9**$^{+/0}$ and a weak shoulder R2 negative of **9**$^{+/0}$. It is known from other spectroscopic methods and from the absence of CV waves due to dtc (*vide supra*) that no decomposition occurs on such a rapid time scale. The only rearrangement recorded is the decoordination of one dtc ligand from **9** to give the 17e radical **9′**, which is stable on the electrochemical time scale. It is also suspected that a solvent molecule rapidly (and reversibly) binds to the 17e metal center to give the 19e state **10**. Thus, we suggest that the two new waves are due to the 17e monodentate form **9′** and the solvent adduct **9***. An additional observation that supports the postulate of a solvent adduct is the fact that anodic oxidation of the 17e species **9′** gives a very reactive 16e species **9′**$^+$. The two ways that **9′**$^+$ can recover the favorable 18e state are (i) by chelating the monodentate dtc ligand, which gives **9**$^+$, and (ii) by binding a solvent molecule to give **9***$^+$. The cationic solvent complex rapidly gives **9**$^+$ and the solvent molecule, but fast cathodic reduction may compete, which leads to the observation of the assigned R2/O3 wave of small intensity. Since the solvent adduct is more electron rich than **9**$^{+/0}$ while **9′**$^{+/0}$ is less electron rich than **9**$^{+/0}$, the wave R0/O1 positive of **9**$^{+/0}$ is attributed to **9′**$^{+/0}$, whereas R2/O3 negative of **9**$^{+/0}$ corresponds to that of the solvent adduct **9***$^{+/0}$.

Scheme 5

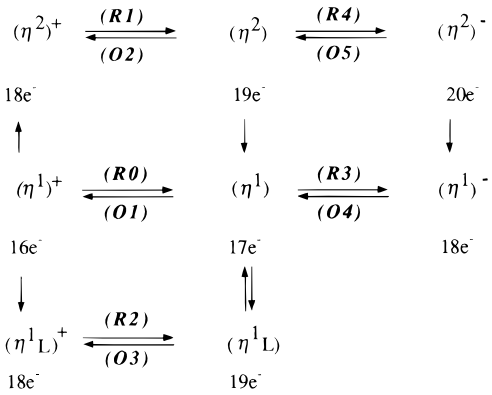

Although these conclusions can be inferred only from the continuous scan of the first zone (left side, Figure 11b), they are well confirmed by the continuous scan of the overall CV shown in Figure 11a. Indeed, in passing from the 19e to the 20e state **9**$^-$, the dtc partial decoordination becomes very exergonic and significantly more rapid (*vide infra*). As expected, the decrease of the wave R1/O2 of **9**$^{+/0}$ is now much more dramatic, and the new waves R0/O1 and R2/O3 exhibit a much higher intensity. It is therefore concluded that the partial decoordination of one dtc ligand is slow but observable at the neutral level **9** on the electrochemical time. On the basis of experiments carried out at a variety of scan rates between 0.02 and 0.8 V s^{-1}, it is estimated that the first-order rate constant for the decoordination of **9** (19e) → **9′** (17e), *k*, is approximately 5 × 10^{-2} s^{-1} at 25 °C. This same process is fast at the anionic 20e level **9**$^-$. The observations of the second zone are fully consistent with these conclusions inferred from the first zone. The cathodic wave **9** → **9**$^-$ is in fact almost totally chemically irreversible. Only a weak shoulder can be observed for the anodic oxidation **9**$^-$ → **9** (O5). A very large wave is apparent on the anodic side (O4) and corresponds to the oxidation of the decoordinated 18e form **9′**$^-$. Also note that the cathodic wave R3 has a significantly reduced intensity. This observation is explained by the fast chelation of **9′** in the course of the full CV scanning which involves oxidation to **9′**$^+$ (*vide supra*). Thus, the overall mechanism for the double monoelectronic process involving partial decoordination of one dtc ligand and subsequent coordination of a solvent molecule to the unsaturated metal center is consistent with a triple-square mechanism (Scheme 5).

Conclusions

(1) The extremely sensitive 17e complex [Fe^{III}Cp*(dtc)CO]$^+$PF$_6$$^-$, **2**$^+$**PF$_6$**$^-$, previously reported in electrocatalytic

studies, has been synthesized from a neutral precursor [Fe^{II}-$Cp^*(\eta^2$-dtc)CO] or [$Fe^{II}Cp^*(\eta^1$-dtc)$(CO)_2$] by one-electron oxidation using $[Fe^{III}Cp_2]^+PF_6^-$. This complex has been characterized by elemental analysis, ESR (rhombic distortion) and Mössbauer spectroscopies, and by its one-electron reduction to the isostructural Fe^{II} complex **2** using the electron-reservoir complex $[Fe^{I}Cp(C_6Me_6)]$.

(2) In $\mathbf{2}^+\mathbf{PF_6}^-$, the CO ligand is extremely labile and is exchanged rapidly by a solvent molecule (MeCN, CH_3COCH_3, CH_2Cl_2) at low temperature to give isoelectronic 17e complexes in which exchange of the solvent by another ligand is facile. Several stable 17e complexes have been synthesized in this way or via ferrocenium oxidation of **1** or **2** and characterized using various spectroscopic techniques and by X-ray crystallography. The 17/18e complexes are new redox couples for which both forms can be isolated using $[Fe^{III}Cp_2]^+PF_6^-$ and $[Fe^{I}Cp(C_6Me_6)]$ as exclusive synthetic redox reagents.

(3) Kinetic studies of ligand exchange in the very substitution labile 17e complexes indicate that 19e intermediates or transition states are involved in associative mechanisms. With dtc as the incoming ligand, 19e species can be isolated and characterized. This reaction ends up by one-electron oxidation of this 19e complex **9** by H_2O to give the 18e cation $\mathbf{9}^+\mathbf{PF_6}^-$ and H_2. A novel series of complexes $[FeCp^*(\eta^2\text{-dtc})_2]^{n+}$, $n = 0$ and 1 ($\mathbf{9}^+\mathbf{PF_6}^-$ and **9**), is accessible via this route.

(4) The cation $\mathbf{9}^+\mathbf{PF_6}^-$ constitutes the first example of an $Fe^{IV}Cp^*$ complex. This is one member of a series of robust compounds which has been characterized by various spectroscopic methods including Mössbauer spectroscopy. The $C_5(CH_2Ph)_5$ derivative has been characterized by X-ray crystallography.

(5) The neutral radical $[Fe^{III}Cp^*(\eta^2\text{-dtc})_2]$, **9**, represents the first example of a 19e complex which has been generated either by addition of dtc^- to a 17e complex or by one-electron reduction of the 18e cationic precursor $\mathbf{9}^+$ (using $[Fe^{I}Cp(C_6Me_6)]$).

(6) Both the 17e and 19e states of the radical **9** have been characterized by ESR, Mössbauer, and NMR spectroscopies and cyclic voltammetry. This is the first example of the concomitant observation of both the 17 and 19e states. MS−SCF−Xα calculations on model compounds for the 17e (**A**) and the 19e (**B**) states of **9** indicate that the two highest occupied levels of **A** are nonbonding with some significant sulfur admixture. On the other hand, the electronic structure of form **B** corresponds to that of a typical authentic 19e system, in which the odd electron occupies an antibonding level of dominant metallic character, with no participation of the π^* dtc orbital.

(7) A triple-square mechanism involving the partial decoordination of the dtc ligand in $\mathbf{9}^{0/-}$ and the coordination of a solvent molecule to the monodentate dtc complexes $\mathbf{9}^{*+/0}$ takes into account the different waves observed by continuous scanning of either the first one-electron reduction zone or the two monoelectronic zones. The 20e species $\mathbf{9}^-$ decoordinates much more rapidly than the neutral form **9** but is still observable on the electrochemical time scale.

Experimental Section

General Data. Reagent-grade tetrahydrofuran (THF), diethyl ether, and pentane were predried over Na foil and distilled from sodium−benzophenone ketyl under argon immediately prior to use. Acetonitrile (CH_3CN) was stirred under argon overnight over phosphorus pentoxide, distilled from sodium carbonate, and stored under argon. Methylene chloride (CH_2Cl_2) was distilled from calcium hydride just before use. All other chemicals were used as received. All manipulations were carried out using Schlenk techniques or in a nitrogen-filled Vacuum Atmospheres drylab. Infrared spectra were recorded with a Perkin-Elmer 1420 ratio recording infrared spectrophotometer which was calibrated with polystyrene. Samples were examined in solution (0.1 mm cells with NaCl windows), between NaCl disks in Nujol, or in KBr pellets. ^{1}H NMR spectra were recorded with a Brucker AC 200 (200 MHz) spectrometer. ^{13}C NMR spectra were obtained in the pulsed FT mode at 50.327 MHz with a Brucker AC 200 spectrometer. All chemical shifts are reported in parts per million (δ, ppm) with reference to the solvent or Me_4Si. Electronic spectra (UV and visible) were recorded at 5 and 25 °C with a Cary 219 spectrophotometer with 10 or 1 mm quartz cells. ESR spectra were recorded with a Brucker ER 200 ttX band spectrometer. Cyclic voltammetry data were recorded with a PAR 273 potentiostat galvanostat. Care was taken in the CV experiments to minimize the effects of solution resistance on the measurements of peak potentials (the use of positive feedback *iR* compensation and dilute solutions ($\approx 10^{-3}$ mol/L) maintained currents between 1 and 10 μA).[25] The additional redox couple ferrocene/ferrocenium was used when possible as a control for *iR* compensation; ΔE_p was 60 mV throughout the experiments. Thermodynamic potentials were recorded with reference to an aqueous SCE in THF (0.1 M $^nBu_4NBF_4$). When necessary, the reference electrode was an Ag quasi-reference electrode (QRE). The silver wire was pretreated by immersion in 10 M HNO_3 for 5 min before use. The counter electrode was platinum. The working electrode was a polished platinum disk embedded in glass (7.85×10^{-3} cm^2) treated first with 0.1 N HNO_3 solution and then with a saturated ammonium iron hexahydrate sulfate solution. The QRE potential was calibrated by adding the reference couple (FcH/FcH^+; FcH = ferrocene). Thermodynamic potentials were recorded with reference to SCE. Mössbauer spectra were recorded with a 25 mCi ^{57}Co source on Rh, using a symmetric triangular sweep mode. Elemental analyses were performed by the Centre of Microanalyses of the CNRS at Lyon-Villeurbanne, France.

Kinetic Studies. The rate of substitution was determined by monitoring the changes in the visible spectra at an appropriate wavelength as a function of time. Isosbestic points were observed (see text). Solutions were prepared at low temperature when required. An adapted system to regulate the temperature was used. Reactions were carried out under pseudo-first-order conditions with respect to the solvent. Pseudo-first-order constants and half-life times were obtained from the slope of a plot of $\ln(A - A_\infty)$ vs. time by least-squares analysis.

X-ray Analyses. A summary of the crystal data collection parameters and structure refinement is given in Table 2. Suitable crystals of **11** and $\mathbf{16PF_6}^-$ were mounted inside thin-walled glass capillaries and sealed under argon and placed at 297(1) K on an Enraf-Nonius CAD-4 diffractometer using graphite-monochromated Mo Kα radiation (λ = 0.710 73 Å) in the $\theta-2\theta$ scan mode. The structures were solved using direct methods and refined using full-matrix least-squares on F^2 with the SHELXTL PC 5.0 software package (Sheldrick, G. M. Siemens Analytical Instruments, 1994). All non-hydrogen atoms were refined with anisotropic thermal parameters. The methyl hydrogens in $\mathbf{16}^+\mathbf{PF_6}^-$ were placed in idealized positions after using a difference electron density synthesis to set the initial torsion angle and refined as a riding−rotating model with general isotropic thermal parameters. All other hydrogen atoms were placed in idealized positions and refined as a riding model with general isotropic thermal parameters. The PF_6^- anion is disordered, and the positions for four of the fluorine atoms were refined with unrestrained anisotropic displacement parameters over two sites with occupation factors of 0.725(18) and 0.275(18). In **11**, the carbon and nitrogen atoms were subjected to "rigid bond" restraints; i.e., the components of the anisotropic parameters in the direction of a bond between two carbon or nitrogen atoms are restrained to be equal within an effective standard deviation of 0.01. This proved to be necessary in order to keep the anisotropic refinement stable.

SCF−MS−Xα Calculations. The standard version of the (spin restricted) density functional SCF−MS−Xα method[35] was used and applied to the 17e and 19e models $[CpFe(\eta^1\text{-}S_2CNH_2)(\eta^2\text{-}S_2CNH_2)]$ (**A**) and $[CpFe(\eta^2\text{-}S_2CNH_2)_2]$ (**B**). Some spin-polarized calculations were also carried out on **B**.[36] The atomic radii of the muffin-tin spheres and the exchange scaling parameters α were taken from the tabulation

(35) Johnson, K. H. *Adv. Quantum Chem.* **1973**, *7*, 143.
(36) (a) Slater, J. C.; Johnson, K. H. *Phys. Rev. B* **1972**, *5*, 844. (b) Slater, J. C.; Wod, J. H. *Int. J. Quantum Chem.* **1971**, *45*, 3.

of Schwartz[37] for heavy elements and from Slater[38] for H. Those relative to the extra molecular (outer-sphere) and the inner-sphere regions are weighted-average values of the atomic ones. The muffin-tin atomic spheres were at first adjusted assuming tangent spheres. In order to provide a better description of the ring systems, the carbon spheres were subsequently enlarged by 25% and an additional empty sphere was located in the center of each ring.[38] The maximum l values in the partial wave expansion included in the calculations were $l = 2$ for Fe and outer spheres, $l = 1$ for S, N, and C spheres, and $l = 0$ for H spheres. SCF calculations were converged to better than ±0.0001 Ry on each level. The geometries considered in the calculations were derived from the experimental structures of related 18e and 17e complexes: [FeCp*(η^1-S_2CNMe_2)$(CO)_2$], **1**,[13] [FeCp*(η^2-S_2CNMe_2)-(PPh_3)], **7**,[13] [FeCp*(η^2-S_2CNMe_2)(CN)], **11**, and [Cp**Fe(η^2-S_2-$CNMe_2)_2$]$^+$, **16**$^+$**PF$_6^-$** (Cp** = η^5-$C_5(CH_2Ph)_5$. Both compounds were idealized to C_s symmetry (pseudo-C_{2v} in the case of **B**). The real symmetry plane of **B** is the one connecting the two dtc ligands. Model **A** was found sterically hindered. Only the conformation shown in Chart 1, with the uncoordinated S-atom lying "down" was found reasonable on steric grounds, in agreement with the X-ray structure of Cp*Fe(η^1-S_2CNMe_2)$(CO)_2$.[13] Unless specified in the text, the major bond distances (Å) and angles (deg) are those listed below. Model **A**: Fe−C = 2.11, Fe−S = 2.28, (η^2-S)−C = 1.72, (η^1-S)−C = 1.76, C(η^2-dtc)−N = 1.32, C(η^1-dtc)−N = 1.34, C−S = 1.65; S−Fe−S = 76, S−C−S = 110, Fe−(η^1-S)−C = 120, (S−C−S) = 125 (η^1-dtc) or 115 (η^1-dtc). Model **B**: Fe−C = 2.17, Fe−S = 2.32, S−C = 1.72, C−N = 1.32; S−Fe−S = 72, S−C−S = 106, Fe−S−C = 91. In both models the C−C, C−H, and N−H bond distances were (Å) 1.42, 1.09, and 1.01, respectively.

Preparation. [FeCp*(η^2-dtc)(CO)]$^+$PF$_6^-$, 2$^+$PF$_6^-$. A 0.764 g sample of complex **1** (2.082 mmol) in 10 mL of THF was stirred with 0.689 g (2.082 mmol) of [$FeCp_2$]$^+$PF$_6^-$ for 15 min, at room temperature, under argon, in the dark. The red solution immediately turned orange with formation of a green precipitate. This precipitate was filtered out in air, washed with 3 × 20 mL portions of dry ether, and dried *in vacuo* (0.925 g; 95% yield). Ferrocene, 0.360 g (93% yield), was also recovered. The green complex could not be crystallized because of its decomposition in solution (*vide infra* for more details). Careful treatment and washings nevertheless provided a satisfactory sample for elemental analysis. Mössbauer data (mm/s vs. Fe at RT (room temperature), 77 K): IS 0.518, QS 0.686. IR (KBr pellet; ν, cm^{-1}): 2030, 1985 (CO); 1550 (CN); 1015 (CS). ESR (solid state sample, 10 K): $g_1 = 2.239$, $g_2 = 2.107$, $g_3 = 2.049$; an evolution of the spectrum with the temperature was observed with an orthorhombic−axial transition at 200 K giving two new g values $g_1 = 2.237$ and $g_{2,3} = 2.071$. Visible (CH_3CN; λ, nm (ϵ, L mol^{-1} cm^{-1}); 5 °C): 584 (811); 452 (2450). Anal. Calcd for $C_{14}H_{21}FeNOPS_2F_6$: C, 34.72; H, 4.37; Fe, 11.53; N, 2.89. Found: C, 34.19; H, 4.36; Fe, 12.11; N, 2.77.

Complex **2**$^+$ could also be isolated as a BF_4^- salt, using the same procedure with [$FeCp_2$]$^+BF_4^-$ (86% yield). IR (KBr pellet; ν, cm^{-1}): 2025, 1985 (CO); 1550 (CN); 1020 (CS). ESR (solid state sample, 12 K): $g_1 = 2.512$, $g_2 = 2.075$, $g_3 = 1.986$. Anal. Calcd for $C_{14}H_{21}$-$FeNOBS_2F_4$: C, 39.46; H, 4.96; N, 3.28. Found: C, 39.75; H, 4.85; Fe, 12.11; N, 2.92.

[FeCp*(η^2-dtc)(CH_3CN)]$^+$PF$_6^-$, 3$^+$PF$_6^-$. A 0.1 g sample of complex **2**$^+$**PF$_6^-$** (0.206 mmol) was introduced under argon into a Schlenk tube. A 10 mL volume of degassed CH_3CN was added, and the mixture was stirred under argon for 10 min at room temperature. The green suspension rapidly gave a bright purple solution. It was then filtered into another Schlenk tube. CH_3CN was then concentrated, and the complex was precipitated by addition of dry ether. The solid was then filtered out under argon on a frit and washed with 3 × 10 mL portions of dry pentane resulting in 89 mg (87% yield) of **3**$^+$**PF$_6^-$**. Mössbauer data (mm/s vs. Fe at RT, 77 K): IS 0.550, QS 0.620. IR (KBr pellet; ν, cm^{-1}): 1535 (CN); 1035 (CS). ESR (CH_3CN, 20 K): $g_1 = 2.611$, $g_2 = 2.184$, $g_3 = 2.001$; (solid state sample, 12 K) $g_1 = 2.672$, $g_2 = 2.007$. Visible (CH_3CN; λ, nm (ϵ, L mol^{-1} cm^{-1}), RT): 514 (1820). Cyclic voltammetry (CH_3CN, 0.1 M ^{n}Bu$_4$NBF$_4$, RT, v = 0.4 V s^{-1}, Pt; $E°$ (V vs. SCE)): 0.570 (ΔE = 60 mV; i_a/i_c = 0.62); +0.835 (ΔE = 120 mV; i_c/i_a = 0.81; α = 0.70; $D = 2.30 \times 10^{-5}$ cm^2 s^{-1}; $k_s = 1.3 \times 10^{-2}$ (±0.1) cm s^{-1}). Anal. Calcd for $C_{15}H_{24}FeN_2$-PS_2F_6: C, 36.23; H, 4.86; N, 5.63. Found: C, 36.48; H, 4.63; N, 5.08.

[FeCp*(η^2-dtc)(THF)]$^+$PF$_6^-$, 4$^+$PF$_6^-$. A 0.1 g sample of complex **2**$^+$**PF$_6^-$** (0.206 mmol) was stirred under argon for 3 h, at room temperature, in CH_2Cl_2/THF (3/1) solution. The mixture slowly assumed the orange color of a clear solution. It was then filtered under argon into another Schlenk tube. The solvent was evaporated, and an orange-brown solid began to precipitate. The precipitation was completed by the addition of dry ether. The resulting solid was then filtered out under argon on a frit and washed with 3 × 10 mL portions of dry pentane (95 mg; 87% yield). IR (THF; ν, cm^{-1}): 1510 (CN); 1020 (CS). ESR (THF, 10 K): $g_1 = 2.323$, $g_2 = 2.050$, $g_3 = 2.004$; (solid state sample, 8 K) $g_1 = 2.313$, $g_2 = 2.037$, $g_3 = 1.990$. Cyclic voltammetry (THF, 0.1 M n-Bu_4NBF_4, RT, v = 0.4 V/s, Pt; $E°$ (V vs. SCE)): −0.248 (ΔE = 75 mV; i_a/i_c = 0.89; $D = 1.07 \times 10^{-5}$ cm^2/s); −0.765 (ΔE = 80 mV; i_a/i_c = 0.88; $D = 1.46 \times 10^{-5}$ cm^2/s).

[FeCp*(η^2-dtc)(L)]$^+$PF$_6^-$ [L = CH_3COCH_3 (5$^+$PF$_6^-$), CH_2Cl_2 (6$^+$PF$_6^-$)]. These complexes were formed by dissolving complex **2**$^+$**PF$_6^-$** in the appropriate solvent giving orange solutions.

5$^+$PF$_6^-$: IR (CH_3COCH_3; ν, cm^{-1}, RT); 1510 (CN); 1015 (CS). ESR (CH_3COCH_3, 20 K): $g_1 = 2.453$, $g_2 = 2.035$, $g_3 = 1.995$. Visible (CH_3COCH_3; λ, nm (ϵ, L mol^{-1} cm^{-1}), RT): 460 (1853).

6$^+$PF$_6^-$: IR (CH_2Cl_2; ν, cm^{-1}, RT): 1515 (CN); 1020 (CS). ESR (CH_2Cl_2, 20 K): $g_1 = 2.571$, $g_2 = 2.135$, $g_3 = 1.990$. Visible (CH_2-Cl_2; λ, nm (ϵ, L mol^{-1} cm^{-1}), RT): 446 (1792).

[FeCp*(η^2-dtc)(PPh_3)]$^+$PF$_6^-$, 7$^+$PF$_6^-$. A 0.3 g sample of complex **2**$^+$**PF$_6^-$** (0.620 mmol) was stirred in 10 mL of either CH_3COCH_3 or CH_3CN with 0.162 g (0.620 mmol) of triphenylphosphine for 30 min, under argon, at room temperature. The resulting purple solution was then filtered through a Celite column (1 cm height) and washed with CH_3CN. Addition of absolute alcohol was followed by a slow recrystallization by evaporation of CH_3CN at ambient temperature. Purple microcrystalline powder **7**$^+$**PF$_6^-$** was isolated in 86% yield (351 mg). Mössbauer data (mm/s vs. Fe at RT, 77 K): IS 0.470, QS 0.659. IR (KBr pellet; ν, cm^{-1}): 1530 (CN); 1015 (CS). ESR (solid state sample, 10 K): $g_1 = 2.478$, $g_2 = 2.238$, $g_3 = 1.960$; an evolution of the spectrum with the temperature was observed with an orthorhombic−axial transition at 100 K giving two new g values of $g_1 = 2.467$ and $g_{2,3} = 2.023$. Cyclic voltammetry (CH_3CN, 0.1 M ^{n}Bu$_4$NBF$_4$, RT, v = 0.4 V/s, Pt; $E°$ (V vs. SCE)): −0.52 (ΔE = 60 mV; i_a/i_c = 1.0; $D = 2.37 \times 10^{-5}$ cm^2/s). Anal. Calcd for $C_{31}H_{36}F_6FeP_2NS_2$: C, 51.82; H, 5.05; Fe, 7.71; N, 1.95; P, 8.62. Found: C, 52.13; H, 5.15; Fe, 7.71; N, 1.93; P, 8.81. Complex **7**$^+$**PF$_6^-$** was also be obtained by stoichiometric oxidation of complex **1** in the presence of 1 equiv of PPh_3 using 1 equiv of [$FeCp_2$]$^+$PF$_6^-$ as oxidant.[10a]

The same procedure was also used to obtain an 80% yield of [FeCp*(η^2-S_2CNEt_2)(PPh_3)]$^+$PF$_6^-$, **10**$^+$**PF$_6^-$**, starting from [FeCp*(η^2-S_2-$CNEt_2$)(CO)]$^+$PF$_6^-$ [10e] and PPh_3 or [FeCp*(η^1-S_2CNEt_2)$(CO)_2$], 1 equiv of [$FeCp_2$]$^+$PF$_6^-$, and PPh_3. Mössbauer data (mm/s vs. Fe at RT, 77 K): IS 0.462, QS 0.631. IR (KBr pellet; ν, cm^{-1}): 1500 (CN); 1015

(37) (a) Schwartz, K. *Phys. Rev. B* **1972**, *5*, 2466; (b) Schwartz, K. *Theoret. Chim. Acta* **1974**, *34*, 225.

(38) Slater, J. C. *Int. J. Quantum Chem.* **1973**, *47*, 533.

(39) (a) Roch, N.; Klemperer, W. G.; Johnson, K. H. *Chem. Rev. Lett.* **1973**, *23*, 149. (b) Weber, J.; Geoffroy, M.; Pénigault, E. *J. Am. Chem. Soc.* **1978**, *100*, 3508. (c) Weber, J.; Goursot, A.; Pénigault, E.; Ammeter, J. H. *J. Am. Chem. Soc.* **1982**, *104*, 1491.

(40) (a) Chambers, J. W.; Baskar, A. J.; Bott, S. G.; Atwood, J. L.; Rausch, M. D. *Organometallics* **1986**, *5*, 1641. (b) Rausch, M. D.; Tsai, W. M.; Chambers, J. W.; Rogers, R. D.; Alt, H. G. *Organometallics* **1989**, *8*, 816.

(41) Hamon, J.-R.; Astruc, D.; Michaud, P. *J. Am. Chem. Soc.* **1981**, *103*, 758.

(42) Brintzinger, H. H.; Palmer, G.; Sands, R. H. *J. Am. Chem. Soc.* **1966**, *88*, 623.

(43) Morrow, J. R.; Astruc, D. *Bull. Soc. Chim. Fr.* **1992**, *129*, 319.

(44) Michaud, P.; Astruc, D.; Ammeter, J. H. *J. Am. Chem. Soc.* **1982**, *104*, 3755.

(45) Astruc, D.; Mandon, D.; Madonik, A. M.; Michaud, P.; Ardoin, N.; Varret, F. *Organometallics* **1990**, *9*, 2155.

(46) Lapinte, C.; Catheline, D.; Astruc, D. *Organometallics* **1984**, *3*, 817.

(47) For ESR data and studies of inorganic and organometallic complexes, see ref 1c, Chapter 4, and the following: (a) Ammeter, J. H. *J. Magn. Reson.* **1978**, *30*, 299. (b) Connelly, N. G.; Geiger, W. E.; *Adv. Organomet. Chem.* **1984**, *83*, 1. (c) Rieger, P. H. In ref 1a, p 270. (d) Baird, M. C. *Chem. Rev.* **1988**, *88*, 1217. (e) Kaim, W. *Coord. Chem. Rev.* **1987**, *76*, 187.

(CS). ESR (solid state sample, 10 K): $g_1 = 2.666$, $g_2 = 2.004$, $g_3 = 1.941$ with an orthorhombic−axial transition at 95 K ($g_1 = 2.663$; $g_{2,3} = 1.977$). Anal. Calcd for $C_{33}H_{40}FeP_2NS_2$: C, 53.08; H, 5.39; Fe, 7.47; N, 1.87; S, 8.58. Found: C, 53.03; H, 5.25; Fe, 7.36; N, 1.91; S, 8.57.

[FeCp*(η^2-dtc)(η^1-dppe)]$^+$PF$_6^-$, 8$^+$PF$_6^-$. A 0.1 g sample of complex **2**$^+$PF$_6^-$ (0.206 mmol) in 10 mL of CH_3CN was stirred with 0.082 g (0.206 mmol) of dppe ((diphenylphosphino)ethane) for 30 min, under argon, at room temperature. The resulting purple solution was then rapidly filtered through a Celite column (1 cm height), concentrated, and recrystallized after the addition of absolute alcohol to give 70 mg (40% yield) of complex **8**$^+$PF$_6^-$. Mössbauer data (mm/s vs. Fe at RT, 77 K): IS 0.445, QS 0.665. IR (KBr pellet; ν, cm^{-1}): 1530 (CN); 1015 (CS). ESR (solid state sample, 10 K): $g_1 = 2.636$, $g_2 = 2157$, $g_3 = 1.975$ with an orthorhombic−axial transition at 110 K ($g_1 = 2.635$; $g_{2,3} = 2.066$). Anal. Calcd for $C_{39}H_{45}FeNP_3S_2$: C, 54.80; H, 5.30; N, 1.65; Fe, 6.13. Found: C, 54.49; H, 5.27; N, 1.61; Fe, 6.00.

[FeCp*(η^2-dtc)(PPh$_3$)], 7.[13] A 0.200 g sample of the cationic precursor **7**$^+$PF$_6^-$ (0.278 mmol) in THF solution was stirred with 0.079 g of [Fe^{I}Cp(C_6Me_6)] (0.278 mmol) for 15 min, under argon. The green solution of the Fe^I complex immediately turned deep red with formation of a yellow precipitate of [FeCp(C_6Me_6)]$^+$PF$_6^-$. The THF was then removed *in vacuo* and the crude product washed 3 times with degassed pentane. Filtration into another Schlenk tube and slow evaporation of the solvent gave 0.130 g (81%) of red-brown microcrystals; 0.093 g (79%) of [FeCp(C_6Me_6)]$^+$PF$_6^-$ was also recovered after filtration through an alumina column and recrystallization. ^{1}H NMR (C_6D_6, 20 °C): δ 7.00 (m, C_6H_5-, 15H); δ 2.27 (s, N(CH_3)$_2$, 6H); δ 1.54 (s, CH_3, 15H). ^{13}C NMR (C_6D_6, 20 °C): δ 201.11 (*C*N); δ 138.61, 135.62, 135.27, 130.15 (C_6H_5-); δ 79.80 (C_5(CH_3)$_5$); δ 37.10 (N(*C*H$_3$)$_2$); δ 10.30 (C_5(*C*H$_3$)$_5$). Mössbauer data (mm/s vs. Fe at RT, 77 K): IS 0.520, QS 2.190. IR (KBr pellet; ν, cm^{-1}): 1480 (CN); 1000 (CS). Anal. Calcd for $C_{31}H_{36}FeNPS_2$: C, 64.91; H, 6.33; Fe, 9.74; N, 2.44; P, 5.40. Found: C, 64.79; H, 6.22; Fe, 9.21; N, 2.44; P, 5.53.

Oxidation of Complex 2 by 1 equiv of [FeCp$_2$]$^+$PF$_6^-$. A 0.062 g sample of the chelate complex **2**, [FeCp*(η^2-dtc)(CO)] (0.183 mmol), in THF solution was stirred under argon with 0.060 g of [FeCp$_2$]$^+$PF$_6^-$ (0.183 mmol) for 30 min. The red-brown solution rapidly turned orange with formation of a green precipitate. The same workup as that described for **1** afforded 0.073 g (83% yield) of complex **2**$^+$PF$_6^-$ and 0.029 g (85%) of ferrocene.

Reduction of 2$^+$PF$_6^-$ by 1 equiv of [Fe^{I}Cp(C_6Me_6)]. An identical procedure to that described for **7** was used for the reduction of a 0.239 g sample of complex **2**$^+$PF$_6^-$. Recrystallization afforded 0.136 g (81%) of complex **2** and 0.186 g (88.6%) of [FeCp(C_6Me_6)$^+$PF$_6^-$. Both complexes were identified by comparison with authentic samples.[9]

[FeCp*(η^2-dtc)$_2$]$^+$PF$_6^-$, 9$^+$PF$_6^-$. A 0.3 g sample of **2**$^+$PF$_6^-$ (0.620 mmol) in 15 mL of oxygen-free CH_2Cl_2 (CH_3COCH_3 or CH_3CN could also be used) was stirred under argon, at 20 °C, with 0.111 g of Nadtc·2H_2O (0.620 mmol) for 1 h. The solution initially assumed the orange color of complex **6**$^+$PF$_6^-$, followed by a blue-ink intermediate color which finally disappeared and gave a bright breen solution. This solution was washed three times with distilled water, dried over Na_2SO_4, and filtered, and complex **9**$^+$PF$_6^-$ was recrystallized at −30 °C overnight (0.254 g; 71%). The aqueous layer containing NaOH was titrated with a 0.01 N solution of HCl according to the stoichiometry of the reaction (69%). The evolution of dihydrogen was monitored by gas chromatography as the reaction proceeded. ^{1}H NMR (CD_3CN, 20 °C): δ 3.228 (s, CH_3, 12H); δ 1.279 (s, CH_3, 15H). ^{13}C NMR: δ 200.56 (*C*N); δ 106.04 (C_5(CH_3)$_5$); δ 38.42 (N(*C*H$_3$)$_2$); δ 9.75 (C_5(*C*H$_3$)$_5$). Mössbauer data (mm/s vs. Fe at RT, 77 K): IS 0.460, QS 0.220. IR (KBr pellet; ν, cm^{-1}, RT): 1540 (CN); 1005 (CS). Cyclic voltammetry (DMF, 0.1 M ^{n}Bu$_4$NBF$_4$, RT, υ = 400 mV/s, Pt; $E°$ (V vs. SCE)): −0.248 ($\Delta E°$ = 60 mV; $i_a/i_c = 0.9$; $D = 1.07 \times 10^{-5}$ cm^2/s; −0.765 ($\Delta E°$ = 70 mV; $i_a/i_c = 0.88$; $D = 1.46 \times 10^{-5}$ cm^2/s). Crystals suitable for X-ray structure determination were obtained, but slow decomposition during data collection permitted only the determination of lattice parameters. This complex crystallizes in a monoclinic system: $a = 12.27$, $b = 17.51$, $c = 13.15$ Å; $\beta = 90.6°$; $V = 2826$ Å^3; $Z = 4$; $d = 1.40$. Anal. Calcd for $C_{16}H_{27}FeN_2PF_6S_4$: C, 33.33; H, 4.72; N, 4.85. Found: C, 33.59; H, 4.71; N, 4.65.

Complex **9**$^+$PF$_6^-$ was also be obtained by slow evolution of a solution of either complex **2**$^+$PF$_6^-$, **7**$^+$PF$_6^-$, or **8**$^+$PF$_6^-$ in either CH_2Cl_2, CH_3COCH_3, or CH_3CN solution in the presence of an excess of water. Neither the action of O_2, prolonged visible photolysis, nor slight warming gave the desired product. The reaction times were dependent on the solvent but generally took between 12 and 24 h. Starting from **2**$^+$PF$_6^-$, the following yields were obtained: 32% (CH_2Cl_2), 37% (CH_3COCH_3), and 30% (CH_3CN). A fraction insoluble in organic solvents consisted of hydrated iron oxides Fe^{III}(O_xH_y) ((0,0) < (x,y) < (3,3)) as shown by IR spectroscopy (KBr pellet; ν, cm^{-1}; RT: 3300 (OH); 1100 (M−OH)) and qualitative tests to determine the oxidation state of iron.[26] ESR spectroscopy revealed an absorption centered at $g = 2.0728$ (ΔH = 1543 G). C_5Me_5H was also recovered in the organic layer and identified by comparison with an authentic sample.

[FeCp*(η^2-dtc)$_2$], 9. The following two procedures were used:

Method A. The same procedure as that described for in **7** was used for the reduction of a 0.200 g sample of [FeCp*(η^2-dtc)$_2$]$^+$PF$_6^-$, **9**$^+$PF$_6^-$, by 1 equiv of [Fe^{I}Cp(C_6Me_6)] at −80 °C in THF solution. Extraction with toluene at −30 °C gave a blue-ink solution already observed during the synthesis of **9**$^+$PF$_6^-$. Further crystallization gave 0.048 g (31%) of the blue complex **9**. Mössbauer data (mm/s vs. Fe at RT, 77 K): see Table 1. IR (KBr pellet; ν, cm^{-1}): 1520 (CN); 1015 (CS). ESR (solid state sample, 12 K): $g_1 = 2.268$, $g_{2,3} = 2.029$. Anal. Calcd for $C_{16}H_{27}FeN_2S_4$: C, 44.54; H, 6.31. Found: C, 45.09; H, 6.63. Similar treatment of the residual solid gave 0.063 g (85%) of [FeCp(C_6Me_6)]$^+$PF$_6^-$ after elimination of black impurities.

Method B. A 0.074 g (4.132 mmol) sample of Na(dtc)·2H_2O was dried *in vacuo* at 80 °C during 48 h, and 0.200 g (4.132 mmol) of complex **2**$^+$PF$_6^-$ was dissolved in CH_3CN. The Na(dtc) salt was then dissolved in the same solvent and added dropwise to the Fe^{III} solution at −40 °C. The bright-purple color of the acetonitrile complex immediately turned blue, and microcrystals formed in the medium. The solvent was then removed by filtration to eliminate the $NaPF_6$ salt. Further crystallization from $CHCl_3$ was carried out and gave 0.134 g (75%) of the desired complex **9**. Different attempts at crystallization failed to yield good-quality crystals for X-ray structure determination.

Study of the Decomposition of Complex [FeCp*(η^2-dtc)(CO)]$^+$PF$_6^-$. In various solvents (CH_3CN, 5 °C; CH_3COCH_3, 5 °C; CH_2Cl_2, 25 °C), 10^{-4} mol/L solutions of the complex were prepared under argon at the desired temperature and immediately examined and monitored by UV visible spectroscopy. As explained in the General Data section the plots $\ln(A - A_\infty)$ vs. time were obtained and gave pseudo-first-order kinetics with half-life times of 5 min (CH_3CN, 5 °C), 13.5 min (CH_3COCH_3, 5 °C), and 57 min (CH_2Cl_2, 25 °C) without any shaking or stirring.

[FeCp*(η^2-dtc)(CN)], 11. A 0.3 g sample of **2**$^+$PF$_6^-$ (0.620 mmol) in 15 mL of oxygen-free CH_3CN (CH_3COCH_3 or CH_2Cl_2 could also be used) was stirred under argon, at 20 °C, for 2 h. A 30 mg amount of NaCN (0.620 mmol) was added and left to react for 12 h. The solution initially assumed the purple color of complex **3**$^+$PF$_6^-$, followed by the red-burgundy color characteristic of the desired complex. The solvent was evaporated *in vacuo*; the crude product was washed with pentane and ether, respectively, and then extracted with freshly distilled and degassed $CHCl_3$. Filtration into another Schlenk tube and concentration of the solvent gave 0.170 g (81%) of a purple microcrystalline powder. Mössbauer data (mm/s vs. Fe at RT): 77 K, IS 0.395, QS 0.884; RT, IS 0.330, QS 0.660. ESR (solid state sample, 4 K): $g_1 = 2.372$, $g_2 = 2.268$, $g_3 = 1.973$. IR (mineral oil; ν, cm^{-1}, RT): 2080 (C≡N); 1510 (CN); 1015 (CS). Cyclic voltammetry (THF, 0.1 M ^{n}Bu$_4$NBF$_4$, RT, υ = 0.4 V/s, Pt $E°$ (V vs. SCE)): −0.842 ($\Delta E°$ = 77 mV; $i_a/i_c = 0.86$; $D = 1.1 \times 10^{-5}$ cm^2/s; E_{pa} = +0.755 V; i_c/i_a = 0). Anal. Calcd for $C_{14}H_{21}FeN_2S_2$: C, 49.85; H, 6.27; N, 8.30; S, 19.01. Found: C, 49.67; H, 6.22; N, 3.17; S, 19.19.

[FeCp*(η^2-dtc)(SCN)], 13. A 0.3 g sample of **2**$^+$PF$_6^-$ (0.620 mmol) in 15 mL of oxygen-free CH_3CN (CH33$COCH_3$ or CH_2Cl_2 could also be used) was stirred under argon, at 20 °C, for 2 h. A 46 mg amount of NH_4SCN (0.620 mmol) was added, and the mixture was left to react for 12 h. The solution initially assumed the purple color of complex **3**$^+$PF$_6^-$, followed by the winy purple color of complex **13** in solution and accompanied by formation of a purple precipitate. The solvent was evaporated *in vacuo*; the crude product was washed with pentane and ether, respectively, and then extracted with freshly distilled and

degassed $CHCl_3$. Filtration into another Schlenk tube and concentration of the solution gave 0.183 g (80%) of a black-purple microcrystalline powder. Mössbauer data (mm/s vs. Fe): 77 K, IS 0.460, QS 0.660; RT, IS 0.389; QS 0.587. IR (mineral oil; ν, cm^{-1}, RT): 2060 (SCN); 1520 (CN); 1015 (CS). ESR (solid-state sample, 3.5 K): $g_1 = 2.483$, $g_2 = 2.088$, $g_3 = 1.997$. Cyclic voltammetry (THF, 0.1 M ^{n}Bu$_4$NBF$_4$, RT, $\upsilon = 0.4$ V/s, Pt, $E°$ (V vs. SCE)): 0.725 ($\Delta E° = 70$ mV; $i_c/i_a = 0.95$; $D = 1.34 \times 10^{-5}$ cm^2/s); −0.740 ($\Delta E° = 90$ mV; $i_a/i_c = 0.80$; $D = 1.38 \times 10^{-5}$ cm^2/s). Cyclic voltammetry (CH_2Cl_2, 0.1 M ^{n}Bu$_4$NBF$_4$, RT, $\upsilon = 0.4$ V/s, Pt; $E°$ (V vs. SCE)): 0.715 ($\Delta E° = 70$ mV; $i_c/i_a = 0.85$; $D = 1.13 \times 10^{-5}$ cm^2/s; $E_{pc} = -0.940$, $i_a/i_c = 0$). Anal. Calcd for $C_{14}H_{21}FeN_2S_3$: C, 45.52; H, 5.73; N, 7.58. Found: C, 45.34; H, 5.72; N, 7.64.

[FeCp*(η^2-dtc)(Cl)], 14. A 0.2 g sample of **2**$^+$**PF$_6$**$^-$ (0.410 mmol) in 10 mL of oxygen-free CH_3CN was stirred under argon, at 20 °C, for 2 h, and 1 equiv of dry NMe_4Cl (0.410 mmol) in CH_3CN solution was then added dropwise at −45 °C over a period of 15 min. The solution was slowly warmed to 20 °C and stirred for one more hour at this temperature. The color of the solution changed from bright-purple to blue-ink. The solvent was evaporated in vacuo; the crude product was washed with pentane and ether, respectively, and then extracted with freshly distilled and degassed $CHCl_3$. Filtration into another Schlenk tube and concentration of the solvent gave 0.115 g (80%) of black pyramidal crystals. IR (mineral oil; ν, cm^{-1}, RT): 2060 (SCN); 1520 (CN); 1015 (CS). ESR (solid-state sample, 2.7 K): $g_1 = 2.277$, $g_2 = 2.169$, $g_3 = 2.061$; with a rhombic transition at 120 K, $g_{1,2} = 2.191$, $g_3 = 2.065$. Cyclic voltammetry (THF, 0.1 M ^{n}Bu$_4$NBF$_4$, RT, $\upsilon = 0.4$ V/s, Pt; $E°$ (V vs. SCE)): +0.562 ($\Delta E° = 65$ mV; $i_c/i_a = 1.00$; $D = 1.32 \times 10^{-5}$ cm^2/s); −0.696 ($\Delta E° = 82$ mV; $i_a/i_c = 0.85$; $D = 5.37 \times 10^{-5}$ cm^2/s). Anal. Calcd for $C_{13}H_{21}FeNS_2Cl$: C, 45.03; H, 6.10; N, 4.04; S, 18.49; Cl, 10.22. Found: C, 44.79; H, 6.07; N, 4.23; S, 18.49; Cl, 10.16.

Acknowledgment. We thank Dr. J. M. Grenèche (Université du Mans) for kindly recording Mössbauer spectra, Dr. J. M. Dance, E. Marquestaut, and B. Barbe (Université Bordeaux I) for ESR and NMR assistance, and the Institut Universitaire de France, the CNRS, the Universities Bordeaux I, Paris VI, and Rennes I, the Région Aquitaine, and the U.S. National Science Foundation (NSF) for financial support. R.D.C. thanks the NSF for a Graduate Research Fellowship.

Supporting Information Available: Text describing X-ray procedures and Tables of X-ray parameters, positional and thermal parameters, bond distances and angles, least-squares planes, and anisotropic thermal parameters of the non-hydrogen atoms for **11** and **16**$^+$**PF$_6$**$^-$ (23 pages). This material is contained in many libraries on microfiche, immediately follows this article in the microfilm version of the journal, can be ordered from ACS, and can be downloaded from the Internet; see any current masthead page for ordering information and Internet access instructions.

JA953603X